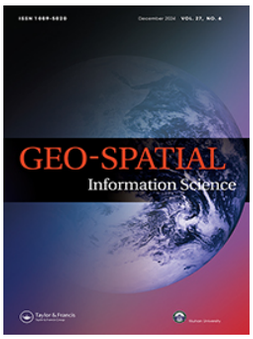

Geo-spatial Information Science

ISSN: (Print) (Online) Journal homepage: www.tandfonline.com/journals/tgsi20

A framework for upscaling aboveground biomass from an individual tree to landscape level and qualifying the multiscale spatial uncertainties for secondary forests

Ye Ma, Jungho Im, Zhen Zhen & Yinghui Zhao

To cite this article: Ye Ma, Jungho Im, Zhen Zhen & Yinghui Zhao (17 Jan 2025): A framework for upscaling aboveground biomass from an individual tree to landscape level and qualifying the multiscale spatial uncertainties for secondary forests, Geo-spatial Information Science, DOI: 10.1080/10095020.2024.2449447

To link to this article: https://doi.org/10.1080/10095020.2024.2449447

GEO-SPATIAL INFORMATION SCIENCE
https://doi.org/10.1080/10095020.2024.2449447

A framework for upscaling aboveground biomass from an individual tree to landscape level and qualifying the multiscale spatial uncertainties for secondary forests

Ye Ma [a,b], Jungho Im [c], Zhen Zhen [a*] and Yinghui Zhao [a*]

[a]Key Laboratory of Sustainable Forest Ecosystem Management-Ministry of Education, School of Forestry, Northeast Forestry University, Harbin, China; [b]Heilongjiang Province Key Laboratory of Geographical Environment Monitoring and Spatial Information Service in Cold Regions, College of Geographical Sciences, Harbin Normal University, Harbin, China; [c]Department of Civil, Urban, Earth, and Environmental Engineering, Ulsan National Institute of Science and Technology, Ulsan, South Korea

ABSTRACT

Secondary forests, a typical forest type in the sub-frigid zone of Northeast China, have significant potential for carbon sequestration. Accurate estimation of the Aboveground Biomass (AGB) of secondary forests and assessment of multiscale uncertainties are crucial for promoting Reduced Emissions from Deforestation and Degradation. This study developed a novel framework to upscale the AGB estimation from the tree to the landscape level and assessed multiscale uncertainties based on multi-platform laser scanning data and Unmanned Aerial Vehicle (UAV) hyperspectral images. The framework included two stages: (1) quantifying multiple uncertainties (uncertainties of individual tree crown delineation, individual tree parameters estimation, and tree species classification) in individual tree-based AGB estimation using Monte Carlo simulations; (2) upscaling the plot to the landscape level estimated AGB using the Nonlinear Simultaneous Equation (NSE) with error-in-variables and quantifying the uncertainties of model residuals, model parameters, and model independent variables. The findings revealed a high accuracy from tree to plot AGB estimation (R^2: 0.75, Root Mean Square Error (RMSE): 6.65 Mg/ha, relative RMSE (rRMSE): 5.40%), with the total and relative uncertainties of 16.85 Mg/ha and 16.29%, respectively, with the highest uncertainty (9.73 Mg/ha) observed in tree species classification. The AGB estimation using NSE achieved an R^2 of 0.69, with an RMSE of 9.91 Mg/ha and an rRMSE of 10.43% from the plot to landscape level; and the uncertainties caused by model parameters, independent variables, and residuals were 5.52 Mg/ha, 14.56 Mg/ha, and 25.25 Mg/ha, respectively, accounting for 3.46%, 24.09%, and 72.45% of the total uncertainty. This study develops a framework for large-scale AGB estimation of mixed forests based on the individual tree approach and uncertainty quantification of multiscale estimates and provides a foundation for precise forestry, sustainable forest management, and carbon neutrality.

ARTICLE HISTORY
Received 21 February 2024
Accepted 31 December 2024

KEYWORDS
Aboveground biomass; secondary forests; individual tree-based approach; uncertainty analysis; nonlinear simultaneous equation

1. Introduction

By absorbing and releasing carbon dioxide, forests are essential to the carbon cycle and the regulation of climate change (Stocker et al. 2013). The quantification of forest carbon stocks is beneficial for the carbon cycle in local and global ecosystems (Asner et al. 2012; Rödig et al. 2019). The forest cover in the region of Heilongjiang Province, China, is about 49%, of which secondary forests account for 70%. Secondary forests contain substantial carbon stocks following years of natural regeneration (Du et al. 2021; Jin et al. 2024). Beyond addressing the need for carbon cycling and balancing, spatial carbon stock estimation in secondary forests would provide extensive social and economic benefits, such as climate change mitigation, biodiversity conservation, and sustainable forestry management (Zald et al. 2016).

Determination of forest carbon stocks typically relies on the Aboveground Biomass (AGB), which can be converted using a biomass expansion factor-based method (Zhao et al. 2019). Remote sensing is a common technique for forest AGB estimation (Chen et al. 2024; Ji et al. 2024; Patel and Majumdar 2011) and is becoming increasingly popular because of its advantages in non-destructiveness, large spatial scale and temporal repeatability. Generally, remote sensing-based forest AGB estimation uses an Area-Based Approach (ABA) (Goldbergs et al. 2018) or Individual Tree-based Approach (ITA) (Zhen et al. 2022). ABA, which can establish a statistical model

CONTACT Zhen Zhen zhenzhen@nefu.edu.cn
*Contributed equally.
Supplemental data for this article can be accessed online at https://doi.org/10.1080/10095020.2024.2449447

between plot- or stand-level AGB and remotely sensed feature variables (e.g. texture features, vegetation index), is currently the primary method for estimating forest AGB at various scales (Yang et al. 2023; Zhang et al. 2022). Numerous studies have demonstrated ABA-based forest AGB for assessing the absorption of carbon dioxide by forests using terrestrial, airborne, and spaceborne remote sensing data (Almeida et al. 2019; Guerra-Hernández et al. 2022; Matasci et al. 2018; Peng et al. 2017; Zald et al. 2016). However, due to the lack of individual tree-level forest properties, it is difficult for ABA to reveal detailed spatial information, which is unfavorable for investigating the spatial uncertainty of AGB estimation at different spatial scales (Qiu et al. 2019). In contrast, ITA can identify and extract individual tree structural parameters (e.g. Diameter at Breast Height (DBH) and tree height) and provide the spatial distribution information. The individual tree AGB can be used as the basis in an up-scaling framework by aggregating AGB estimations from individual trees to stand level (Zhen et al. 2022).

In ITA-based AGB estimation, Individual Tree Crown Delineation (ITCD) is usually performed first, based on which the parameters of individual trees are estimated, and AGB is calculated using the allometric growth equation (Zhen et al. 2022). Therefore, an accurate ITCD algorithm, tree species classification algorithm (for mixed forests), and accurate parameter estimation are indispensable in an ITA framework. Various algorithms have been developed for ITCD, such as the marker control watershed algorithm based on the canopy height model (Navarro et al. 2020) and comparative shortest-path algorithm based on 3-D point clouds (Tao et al. 2015). The improvement of traditional or novel algorithms enables individual trees to be delineated under heterogeneous secondary forests, particularly when aided by LiDAR data (Zhen et al. 2022). In the case of mixed secondary forests, the tree species classification is a prerequisite for ITA-based AGB estimation because incorrect classification can lead to the incorrect application of the allometric growth equation. The recent collaboration of UAV hyperspectral imagery with high spatial-spectral resolution and Unmanned Aerial Vehicle Laser Scanning (ULS) data with high point cloud density has provided outstanding data sources for tree species classification (Brovkina et al. 2018; Qin et al. 2022; Quan et al. 2023). The expeditious advancement of Convolutional Neural Networks (CNNs) has notably enhanced the accuracy of tree species classification compared to conventional machine learning models (e.g. random forest) (Sothe et al. 2020). CNNs have evolved toward deeper convolutional structures with the emergence of algorithms such as Resnet50 and Resnet101 (He et al. 2016). Ultra-deep CNNs can provide more abstract features for distinguishing tree species. In addition, a suitable and advanced data source is required to estimate individual tree parameters accurately. In recent years, near-ground remote sensing techniques such as Terrestrial Laser Scanning (TLS) have been employed to obtain complete three-dimensional (3-D) trunk and canopy structural information, which is promising for precise ITCD and DBH estimations in the understory of secondary forests (Brede et al. 2022). Overall, it is worth exploring how to effectively combine multiple data sources, ITCD algorithms, and tree-classification algorithms to improve ITA-based AGB estimation accuracy, especially in mixed secondary forests with complex stand structures.

Furthermore, it is imperative to understand the uncertainty of landscape AGB estimation and how errors propagate from the individual tree to the landscape level. Uncertainty is typically defined as variability in measurements or other areas, and standard deviation and coefficients of variation are utilized to quantify the variability of model and remote sensing procedures for AGB estimates (Chen, Laurin, and Valentini 2015). The uncertainty of ITA-based AGB estimation consists of uncertainties from the allometric growth equation (e.g. model parameters, residuals, and independent variables), ITCD, individual tree parameter estimation, and tree species classification (in the case of mixed forests). Monte Carlo (MC) simulations (Chen, Laurin, and Valentini 2015), Taylor expansions (Gertner, Cao, and Zhu 1995), and polynomial regressions (Gertner, Parysow, and Guan 1996) are the standard methods for quantifying these uncertainties. Although researchers have incorporated multiple uncertainties (e.g. allometric growth equation and individual tree parameters) into RS-based AGB estimation uncertainty (Persson, Ekström, and Ståhl 2022; Xu et al. 2018; Zhen et al. 2022), they have not fully investigated and comprehensively assessed multiscale AGB estimation and its uncertainty under the ITA framework (i.e. uncertainty of ITCD and tree species classification), especially for mixed secondary forests. In addition, when tree-level estimates are upscaled to plot- and landscape-level AGB estimation, there are various error propagations, such as the errors of the AGB estimation model and the error of the independent variable. Only a few studies have examined certain aspects of these errors from multiple sources (Chen, Laurin, and Valentini 2015). Therefore, it is vital to determine how to estimate large-level AGB by the ITA framework and assess the uncertainty in this process.

This study aimed to develop a nondestructive AGB estimation and uncertainty assessment framework through ITA and to establish an up-scaling AGB estimation model and error propagation framework from the plot to landscape level in secondary forests. For this purpose, the objectives of this study include (1)

develop a framework for ITA-based AGB estimation at the individual tree level and explore the optimal ITCD and tree species classification algorithms in secondary forests using TLS, ULS, and UAV hyperspectral data, (2) quantify the uncertainty in the ITCD algorithm, individual tree parameter estimation, and tree species classification using MC simulation from the tree- to plot-level, and (3) develop an upscaling AGB estimation model from the plot to landscape level and evaluate the uncertainty of multiscale AGB estimation.

2. Materials

2.1. Study area

The study area is situated in the Maoershan experimental forest farm, Shangzhi City, Heilongjiang Province China (Figure 1), with a total area of 264.08 km^2. Maoershan forest farm has an average altitude of 300 m and a continental monsoon climate. Owing to the destruction of forests, the original vegetation has reversed succession, forming the current distribution of the mixed secondary forests with other plantations. According to the forest resources inventory data in 2015, broadleaf mixed forests and coniferous-broadleaf mixed forests accounted for about 65%, larch (*Larix olgensis* Henry) plantations accounted for about 12%, and other plantations (i.e. Korean pine (*Pinus koraiensis* Sieb. et Zucc.), white birch (*Betula platyphylla* Suk.), elm (*Ulmus pumila* L.)) accounted for approximately 17%.

2.2. Data and preprocessing

2.2.1. Field inventory data

Fifty mixed-forest plots (30 m × 30 m) dominated by the main tree species were surveyed during the summers of 2021 and 2022. In total, 4527 trees (DBH ≥ 5 cm) were measured and recorded, including the DBH (cm), tree height (m), tree species, and location. Tree position was measured using a real-time kinematic Global Positioning System receiver, with a positional error of less than 5 cm. The statistics of measured parameters was described in Table 1. Species-specific additive biomass equations were applied to calculate the reference AGB of individual trees (Dong, Li, and Song 2015; Dong, Zhang, and Li 2015). The parameters of additive biomass equations were listed in the Supplementary Table S1.

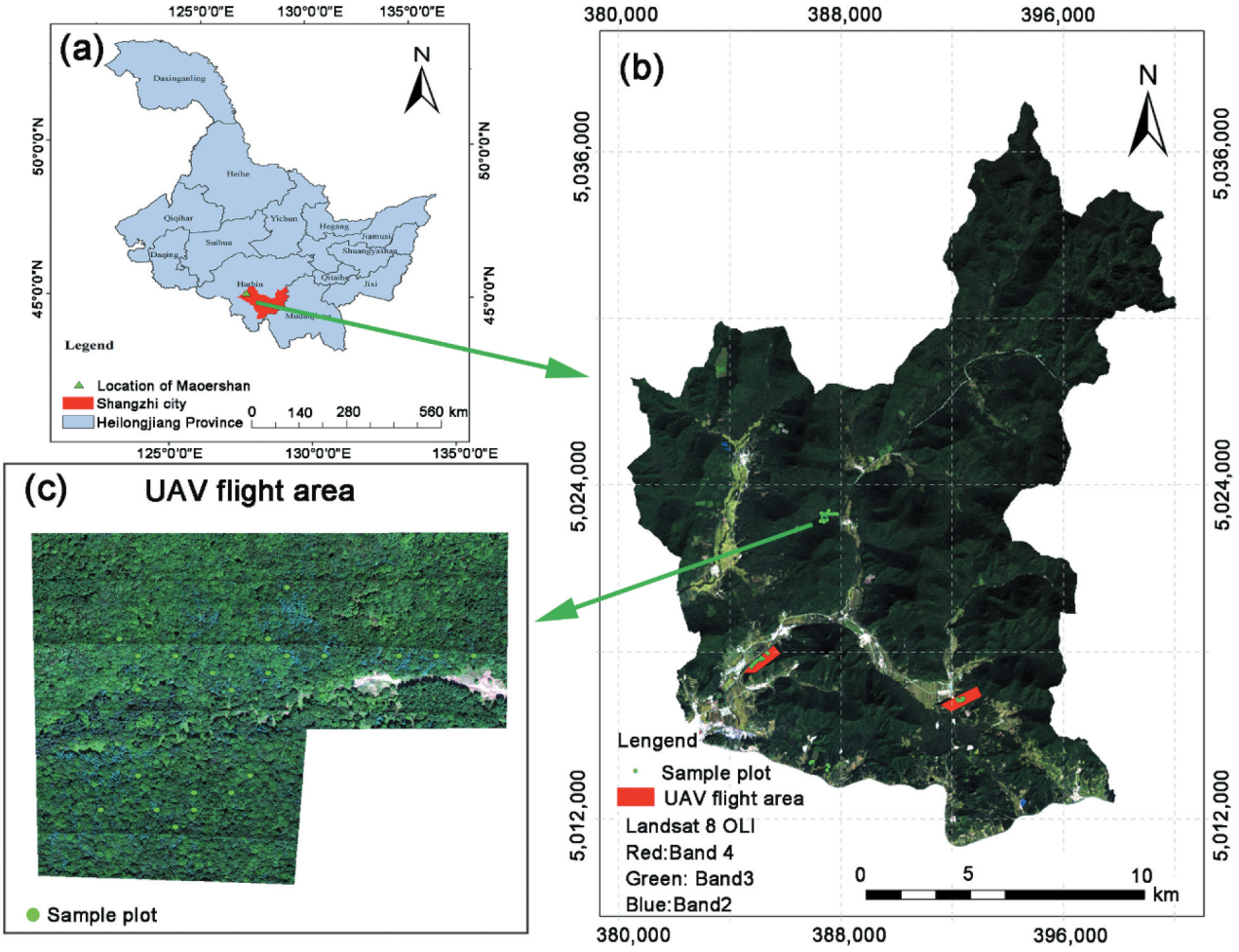

Figure 1. Location of the study area: (a) location of Heilongjiang Province; (b) location of Maoershan forest farm. The base map is Landsat 8 OLI optical imagery with true color; (c) example of a UAV flight region with sample plots and hyperspectral imagery.

Table 1. Descriptive statistics of field inventory data.

		DBH (cm)					Height (m)				
Species	*N*	Max	Median	Min	Mean	STD	Max	Median	Min	Mean	STD
Korean pine (KP)	2556	48.3	13.8	5.0	14.9	6.1	25.5	11.5	4.1	11.9	3.6
White birch (WB)	263	33.1	18.7	6.3	19.0	5.5	28.7	16.7	7.0	16.7	4.1
Elm (EL)	438	45.4	14.6	5.4	16.4	7.1	25.0	14.1	4.5	14.1	4.4
Manchurian ash (MA)	258	50.5	24.1	7.5	24.6	7.4	26.0	18.3	7.5	18.1	3.6
Manchurian walnut (MW)	218	50.8	20.8	6.8	21.1	7.1	30.3	18.7	7.5	18.6	3.9
amur cork-tree (AC)	37	47.8	19.0	11.5	21.1	7.6	25.8	15.5	10.5	15.9	3.3
Acer mono (AM)	136	35.6	12.2	6.2	14.6	6.2	24.2	12.8	4.6	13.0	3.7
Populus (PO)	128	63.0	17.7	6.3	21.9	12.1	33.3	18.0	6.9	18.2	4.9
Other tree species (OT)	493	22.7	18.3	5.8	15.2	6.8	26.4	14.9	5.7	15.1	3.5

Other tree species, including Padus avium, Mongolian oak, Camphor pine, and Larch.

2.2.2. Optical imagery and preprocessing

In this study, a Reson Pika L hyperspectral sensor on a DJI M600 pro UAV was used to acquire the UAV-borne Hyperspectral Images (U-HSIs). An area of 2 km^2 was covered by U-HSIs in August 2021 and 2022 without any clouds. It is composed of 150 bands ranging from 400 nm to 1000 nm. The high spatial–spectral resolution (0.5 m and 4 nm, respectively) sensor was used to achieve accurate discrimination among tree species. Geometric correction, geographic alignment and generation of hypercubes were performed to acquire the actual reflectance using the MegaCube software (http://www.iris-rs.cn/).

The forest area was extracted by Landsat 8 OLI image acquired on 24 July 2020 (product ID: LC81170292020206LGN00). The Landsat 8 OLI imagery was preprocessed to obtain surface reflectance, including radiometric calibration, atmospheric correction and terrain correction, and was geographically aligned with Airborne Laser Scanning (ALS) data using the ENVI 5.2 software.

2.2.3. LiDAR data and preprocessing

Three LiDAR datasets (TLS, ULS, and ALS) were used to explore the uncertainty from tree-, plot-, and landscape-level AGB estimations. The TLS and ULS data were employed to tree-plot AGB estimation and uncertainty analysis, whereas the ALS data were employed to landscape AGB estimation and uncertainty analysis.

In August 2021 and 2022, terrestrial laser scanner of the RIEGL VZ-400i was employed to conduct comprehensive scans of the 50 sample plots. Based on the density of trees in the sample plots, 10–15 TLS scanning stations were established for each sample plot. The DJI M600 pro UAV was utilized to collect ULS data for August 2021 and 2022, covering the same area as the U-HSIs, with an approximate total area of 2 km^2. The ALS data were obtained in September 2015 using a LiCHy airborne observation system. The average point density of ALS, ULS, and TLS were 7 pts/m^2, 270 pts/m^2, and 1.5×10^5 pts/m^2, respectively. Supplementary Table S2 displays the additional key parameters for the three LiDAR datasets.

The preprocessing of ULS, TLS, and ALS data involved the following steps: (1) applying noise filtering; (2) classifying ground point using improved progressive triangular irregular network densification (Zhao et al. 2016); (3) normalizing point clouds to obtain the vegetation height; and (4) creating Canopy Height Model (CHM) with spatial resolution of 0.5 m based on normalized point clouds using TIN interpolation.

The iterative closest point algorithm was employed to re-register the TLS to ULS data to obtain the entire canopy vertical structure (Besl and McKay 1992). Fused ULS-TLS (hereafter, U-TLS data) point cloud data were applied to ITCD. All preprocessing of the LiDAR data was conducted using LiDAR 360 software V5.2 (https://www.lidar360.com/).

3. Methods

3.1. Overview of methodology

To develop a multiscale nondestructive AGB estimation and uncertainty assessment framework, the methodology included (1) comparing different algorithms and different data sources for tree species classification and selecting the optimal combination for AGB estimation from the tree to plot level; (2) quantifying multiple uncertainties in ITA-based AGB estimation using MC simulation (Raychaudhuri 2008), including in the ITCD algorithm, individual tree parameter estimation, and tree species classification; (3) establishing an ALS-based AGB upscaling model from the plot to the landscape level based on NSE and assessing the uncertainty in the components of the model based on error propagate principles. A flowchart of the study is displayed in Figure 2.

3.2. Individual tree-based AGB estimation

3.2.1. Individual tree parameters estimation (ITPE)

Accurate individual tree crown delineation is vital for parameters estimation and tree species classification. In this study, the U-TLS data were applied to

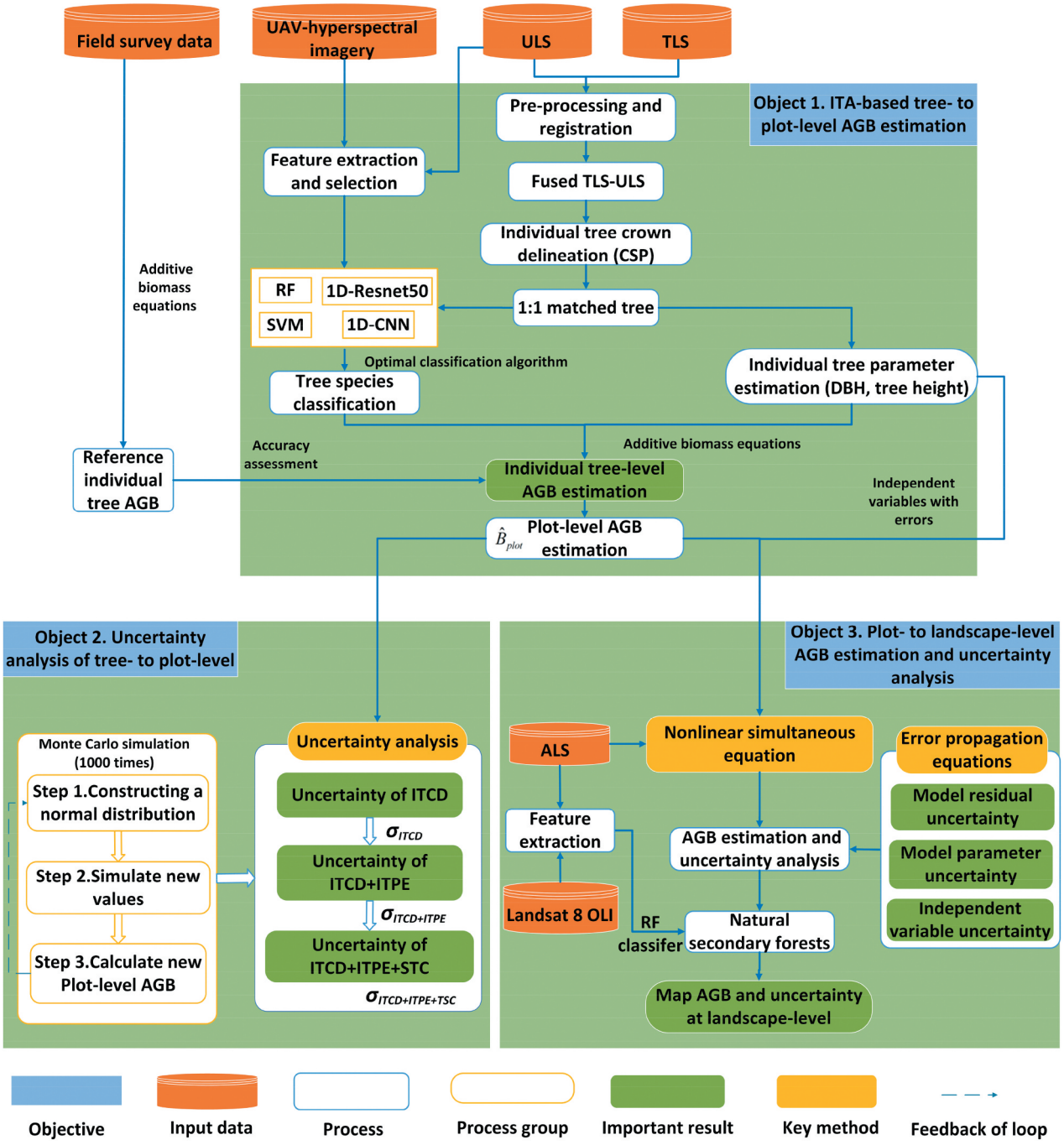

Figure 2. Process flow proposed in this study.

the comparative shortest-path algorithm with seed points (Tao et al. 2015) for segmenting individual trees because the fused U-TLS data effectively address the issue of suppression of lower trees by the upper trees (Huo, Lindberg, and Holmgren 2022). Seed points were generated using the least-squares algorithm to fit the cylinder of the point cloud at a height of 1.3 m.

The accuracy of the ITCD algorithm was assessed using three indices: recall (r), precision (p), and F-score (Li et al. 2012). Following Kaartinen et al. (2012), we considered the location and attribute relationship (i.e. DBH) of the detected and reference trees and defined a 1:1 matched tree as follows:

(1) Search all detected treetops within each reference crown for an initial match;
(2) Calculate the mean difference in DBH between the reference and detected trees according to the initially matched trees from step (1);
(3) If only one detected treetop exists in the reference crown and its DBH difference is less than the mean difference of the DBH in step (2), the detected tree is considered a 1:1 match.

The tree height from CHM was determined by identifying the local maximum height within 1:1 matched tree crown. The DBH was estimated at 1.3 m height of point cloud data using the nonlinear least-squares

fitting circle algorithm (Gander, Golub, and Strebel 1994). The coefficient of determination (R^2), RMSE and rRMSE were adopted to assess the accuracy of individual tree parameter estimation.

3.2.2. Tree species classification

Based on field survey data, the classification system of eight major tree species (groups) was established, and sample sizes were determined based on 1:1 matched trees, including Korean pine, white birch, three hardwood trees (i.e. Manchurian ash, Manchurian walnut, and Amur corktree (*Phellodendron amurense* Rupr.)), elm, Populus, Acer mono, and other broadleaf trees (e.g. Tilia amurensis (*Tilia amurensis* Rupr.), Mongolian oak). Sample sizes for each category are shown in Supplementary Table S3. The features extracted from U-TLS and U-HSIs are displayed in Supplementary Table S4 and Table S5, respectively. To address the "black box" issue in machine learning models, we employed an interpretable machine learning technique (i.e. SHapley Additive exPlanations (SHAP) (Molnar 2020), which assesses the global and local importance of features in a given machine learning model.

To compare the performance of classic machine learning and deep learning models, four models, RF (Amini et al. 2018; Hartlinga, Sagan, and Maimaitijiang 2021), SVM (Mountrakis, Im, and Ogole 2011), 1D-CNN (Zhao et al. 2022), and 1D-Resnet50 (He et al. 2016), were compared based on the different data sources: U-HSIs, U-TLS, and U-HSIs+U-TLS. 1D-CNN and 1D-Resnet50 were used in order to explore the impact of DL models with different architectures on tree species classification. The 1D-CNNs adopted six convolutional layers with a kernel size of three, and every two convolutional layers were connected with a maximum pooling layer of size three. The Resnet algorithm cleverly introduces a residual module, which avoids the problem of gradient disappearance and allows Resnet to train a thousand-layer network (He et al. 2015). The Resnet-50 has four groups of blocks, each with three, four, six, and three bottlenecks, respectively (Figure 3). In this study, a one-dimensional convolution was used for all convolution layers to reduce the manual error of creating image samples in a 2D-CNN and circumvent the challenge of small image sizes in tree species

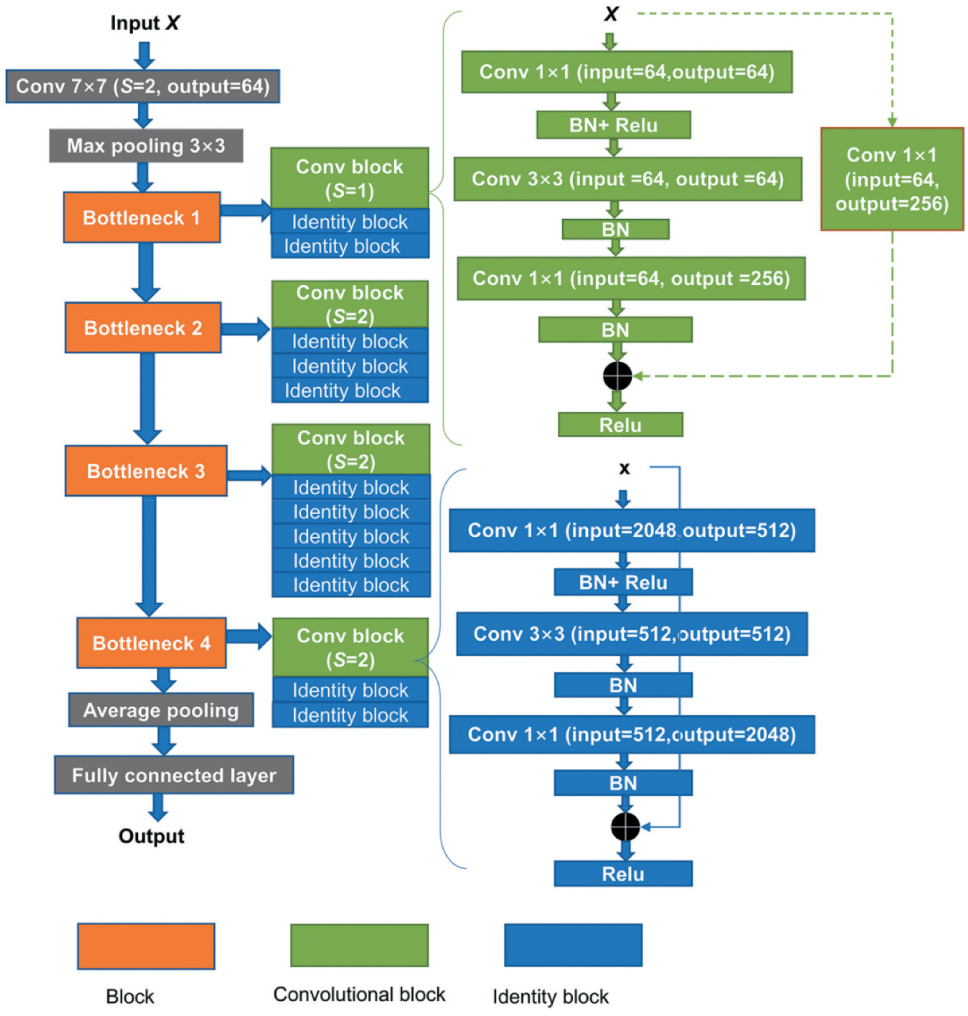

Figure 3. Resnet-50 network structure. The green/blue bottleneck in different blocks has the same convolution module but the number of input and output channels are different; the first bottleneck in Block 1 has a stride of 1 and the first bottlenecks in the rest blocks have a stride of 2. Note: *S* is stride; BN is batch normalization; *X* represents independent variables.

classification (Xi et al. 2021). The hyperparameters of all four algorithms were optimized using random searches (Bergstra and Bengio 2012), and shown in Supplementary Table S6.

The training set (70% of the dataset) was used for model training based on stratified 10-fold cross-validation: using tree species classes as strata, which can effectively avoid bias in model evaluation owing to unbalanced data distribution (Diamantidis, Karlis, and Giakoumakis 2000). The test set (30%) was used to assess classifications using three metrics: the User's Accuracy (UA), Producer's Accuracy (PA), and Overall Accuracy (OA). All algorithms were implemented using Python 3.7 and the sklearn1.0+tensorflow1.14 package.

3.2.3. Individual tree-based plot-level AGB estimation

The AGB (kg) of individual trees was estimated using the estimated DBH and tree height, and optimal tree species classification results (only 1:1 matched trees adopted). The plot-level AGB (Mg/ha) was summed by all individual tree-based AGB in sample plot and assessed using R^2, RMSE, rRMSE, and bias between the estimated and reference plot AGB.

3.3. Uncertainty analysis of individual tree-based AGB estimates from individual tree to plot-level

3.3.1. Uncertainty of individual tree crown delineation

Inaccurate ITCD is the root cause of the uncertainty in ITA-based AGB estimates. Since the goal of this study was to examine the uncertainties associated with AGB estimation, which are derived from automatic individual tree detection for landscape-level estimation, only the results from an automatic ITCD with a detection view were considered. In other words, from a detection view, only the correct segmentations (TP or 1:1 matched trees) and commission errors (over segmentations or FP) were visible. However, the omission errors (under segmentations or FN) generated from a reference view were not considered. Thus, an MC procedure that determined the uncertainty of ITCD (including TP and FP) was conducted as follows:

Step 1. New TP and FP were generated according to two normal distributions. The mean and variance of TP and FP for the 50 plots are as follows:

$$\begin{cases} TP' \sim N\left(\overline{TP}, VAR_{TP}\right) \\ FP' \sim N\left(\overline{FP}, VAR_{FP}\right) \end{cases} \tag{1}$$

where $TP'$and $FP'$are the number of simulated correctly detected and over-segmented individual tree through the normal distribution; $\overline{TP}$ and $\overline{FP}$ are the mean of 50 sample plots of correctly detected and over-segmented individual tree, respectively; VAR_{TP} and VAR_{FP} are the variance of 50 sample plots of correctly detected and over-segmented individual tree, respectively.

Step 2. A number of simulated individual trees (i.e. TP' and FP') were randomly selected from the reference trees in each sample plot according to Equation (1), and the plot AGB was summed by the tree AGB.

$$\widehat{B}_{plot} = \sum_{i=1}^{TP'} \widehat{B}_i + \sum_{j=1}^{FP'} \widehat{B}_j \tag{2}$$

where $\hat{B}_{plot}$ is a simulated plot-level AGB, and $\hat{B}_i$ and $\hat{B}_j$ are the AGBs of the correctly segmented and over-segmented individual trees, respectively.

Step 3. By iteratively performing steps 1 and 2 k times, the mean, the standard deviation (i.e. the uncertainty of the ITCD), and coefficient of variation (relative uncertainty) of the plot-level AGB were calculated according to Equation (3).

$$\begin{cases} \bar{B}_\psi = \frac{1}{k}\sum_{i=1}^{k} \hat{B}_i \\ \sigma_\psi = \sqrt{\frac{1}{k}\sum_{i=1}^{k} \left(\hat{B}_i - \bar{B}_\psi\right)^2} \\ cv_\psi = \frac{\sigma_\psi}{\bar{B}_\psi} \end{cases} \tag{3}$$

where k is simulation times (i.e. $k = 1000$ in this study), $\widehat{B}_i$ is the plot AGB value of the ith simulation, $\bar{B}_\psi$ is the mean plot AGB of the k times simulation, σ_ψ and cv_ψ are the standard deviation and the coefficient of variation of the simulated plot-level AGB, respectively. At this point, only the uncertainty of ITCD was included, therefore $\psi = \{ITCD\}$. The uncertainties in individual tree parameter estimation and tree species classification were not considered because the actual DBH, tree height, and tree species were used.

3.3.2. Uncertainty of individual tree crown delineation and parameters estimation

The uncertainty of ITCD and individual tree parameter estimation in AGB estimation refers to the uncertainties of automatic ITCD and parameters estimation. Based on the ITCD results, the MC simulation procedure for individual tree parameter estimation uncertainty was conducted as follows:

Step 1. To quantify the uncertainty of individual tree parameters in AGB estimation, the normal distributions of random errors were constructed to simulate a new DBH and tree height. Assuming that the mean of the distribution is zero and standard deviation is the residual of the estimated DBH and tree height, as shown in Equation (4):

$$\begin{cases} \varepsilon_D' \sim N\left(0, \varepsilon_D^2\right) \\ \varepsilon_H' \sim N\left(0, \varepsilon_H^2\right) \end{cases} \tag{4}$$

where ε_D^2 is the residuals of the estimated DBH; ε_H^2 is estimated tree height; $\varepsilon_D^{'}$ is the random errors derived from the DBH and $\varepsilon_H^{'}$ is the random errors derived from tree height.

Step 2. The new DBH and tree height were simulated and generated based on the new random errors in step 1, as follows:

$$\begin{cases} D' = D + \varepsilon_D^{'} \\ H' = H + \varepsilon_H \end{cases} \quad (5)$$

where D is the estimated DBH; H is estimated tree height; D' is the newly simulated DBH; H' is the newly simulated tree height.

Step 3. New AGBs of individual trees were calculated according to the simulated DBH and tree height and aggregated to obtain the simulated plot AGB. The mean plot-level AGB of 1000 simulations and the uncertainty of the simulation were calculated using Equation (3), where $\psi = \{ITCD + individual\ tree\ parameter\ estimation\}$. The uncertainty of the tree species classification was not included because the actual tree species were applied.

3.3.3. Uncertainty of individual tree crown delineation, parameters estimation, and tree species classification

Figure 4 shows a diagram of the different cases of the tree species classification simulation from a detection perspective. Based on the results of the ITCD algorithm, a subset of trees was randomly selected and simulated to accurately classify trees from each sample plot (Figure 4(a)). For incorrectly classified individual trees (Figure 4(b)), a tree species was randomly assigned in order to simulate classification errors. Because over segmented trees (Figure 4(c)) had no labels for classification, the type of the trees was predicted using the classification model.

The MC simulation used to quantify the uncertainty of the tree species classification was conducted as follows:

Step 1. Two normal distribution functions were constructed as follows:

$$\begin{cases} OA^{'} \sim N(\overline{OA}, VAR_{OA}) \\ error^{'} \sim N(\overline{error}, VAR_{error}) \end{cases} \quad (6)$$

where *OA'* and *error'* are the simulated OA and error of tree species classification, respectively; *OA* and *error* are the means of the OA and error (i.e. 1-OA) in the 50 sample plots, respectively; and VAR_{OA} and VAR_{error} are the variances of OA and error, respectively.

Step 2. According to the normal distribution, two parts of individual trees (correctly classified and incorrectly classified from a user's perspective) were randomly selected, and the individual tree AGBs were summed to obtain a plot AGB.

Step 3. Repeat steps 1 and 2 for 1000 times using the MC simulation Equation (3), where $\psi = \{ITCD + individual\ tree\ parameter\ estimation + tree\ species\ classification\}$ to obtain a simulated plot-level AGB estimate with uncertainties in the ITCD, individual tree parameter estimation and tree species classification procedures. The MC simulation program was implemented using the Numpy and Scipy libraries in python.

3.4. Plot-level to landscape AGB estimation

3.4.1. Extraction of the secondary forests

To distinguish secondary forests from other plantations, ALS and Landsat 8 OLI were used to extract mixed secondary forests using the random forest model, which has been widely used and performed well in classifications (Cheng and Wang 2019; Liu et al. 2018). The 101 and 96 features were extracted from ALS (Supplementary Table S4) and Landsat 8

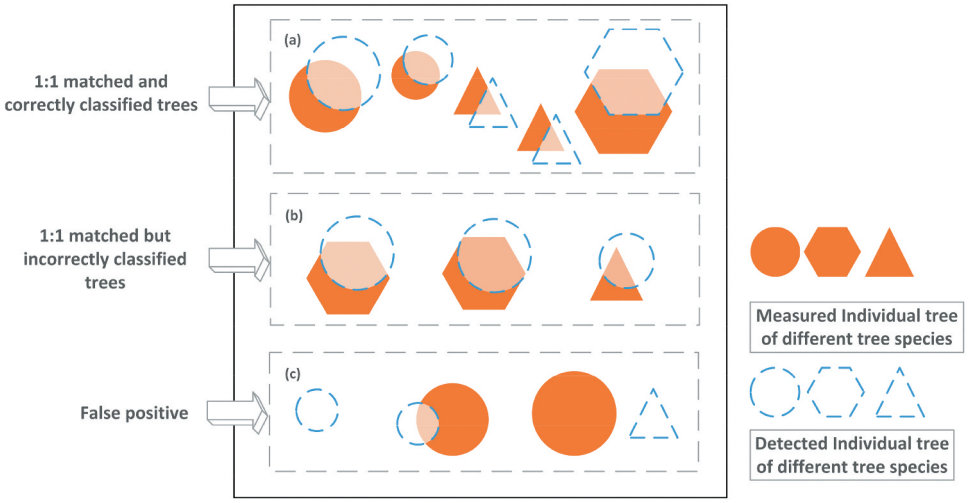

Figure 4. Diagram of the different cases for tree species classification simulation from the detection perspective: (a) 1:1 matched and correctly classified trees; (b) 1:1 matched but incorrectly classified trees; (c) false positive.

OLI (Supplementary Table S7), respectively. The classification system and sample sizes applied for the extraction of the secondary forests are shown in Supplementary Table S8 based on a stratified sampling method (70% of samples as training data, 30% as testing data). Uncertainty and AGB at the landscape level were mapped using *GDAL* library in python.

3.4.2. Establishment of nonlinear simultaneous equation for landscape-level AGB estimation

Based on ALS data that cover the Maoershan Forest Farm, the plot AGB was extrapolated up to the landscape level through the nonlinear error-in-variable model (Tang, Li, and Wang 2001). An error-in-variable model refers to a linear or nonlinear model with variable set that is subject to errors, whereas the remaining variables are error-free.

The model is referred to as an NSE (Tang, Li, and Wang 2001) when the number of equations equals the number of error-in variables. In this study, the NSE model was established to connect plot-level with landscape-level AGB estimates as follows:

$$\begin{cases} H_{ALS} = a_1 + b_1 \cdot H + c_1 \cdot D + \varepsilon_1 (\text{Model I}) \\ D_{plot,ITA} = a_2 + b_2 \cdot H_{ALS} + \varepsilon_2 (\text{Model II}) \\ B_{plot,ITA} = a_3 {H_{ALS}}^{b_3} \cdot {D_{plot,ITA}}^{c_2} + \varepsilon_3 (\text{Model III}) \end{cases} \tag{7}$$

where D is the measured plot DBH, H is the measured tree height and are considered error-free variables; H_{ALS} is the canopy height extracted from ALS-generated CHM and is considered an error-in-variable; $D_{plot,\ ITA}$ and $B_{plot,ITA}$ are the plot-level DBH and AGB based on ITA, respectively, and are considered error-in-variables. a_i, b_i, c_i ($i = 1,2,3$) are the model parameters to be fitted. ε_i ($i = 1,2,3$) are model residuals. Models I and II were developed to estimate plot-level canopy height and DBH, respectively, and Model III was designed to estimate landscape-scale AGB using plot-level canopy height (H_{ALS}) and DBH ($D_{plot,ITA}$), which were the response variables of Models I and II.

To quantify the AGB estimation errors of the parametric models, the following sources of error were considered: (1) errors due to incorrect fitting of model parameters, (2) errors in the independent variables (i.e. H_{ALS}, $D_{plot,ITA}$, $B_{plot,ITA}$), and (3) errors caused by model residual variability. Assuming that these three errors are independent, the total uncertainty of AGB estimation can be expressed according to the error propagation principle (Merrin 2017) as follows:

$$\sigma_{t,\ plot} = \sqrt{{\sigma^2}_{f,\ plot} + {\sigma^2}_{x,\ plot} + {\sigma^2}_{\varepsilon,\ plot}} \tag{8}$$

where $\sigma_{t,\ plot}$ represents the total model uncertainty; $\sigma_{f,\ plot}$, $\sigma_{x,\ plot}$ and $\sigma_{\varepsilon,\ plot}$ are the standard deviation of the model parameters, independent variables and model residuals, respectively.

Based on a linear approximation, the uncertainty of the model parameters can be calculated as follows (Chen, Laurin, and Valentini 2015):

$${\sigma^2}_{f,plot} \approx \sum_{j=1}^{p} \sum_{k=1}^{p} \frac{\partial f}{\partial \beta_j} \frac{\partial f}{\partial \beta_k} \operatorname{cov}(\hat{\beta}_j, \hat{\beta}_k) \tag{9}$$

where p is the number of parameters; $\frac{\partial f}{\partial \beta_j}$ and $\frac{\partial f}{\partial \beta_k}$ are the partial derivative of the parameters, and $\operatorname{cov}(\hat{\beta}_j, \hat{\beta}_k)$ is the variance-covariance matrix of the parameter estimates.

For the uncertainty of the independent variables, the error propagation of the multivariate model can be represented as follows (Merrin 2017):

$$\begin{aligned} \sigma^2_{x,plot} = & \sum_{i=1}^{m} \left(\frac{\partial f}{\partial x_i} \right)^2 \operatorname{var}(x_i) \\ & + 2 \sum_{i=1}^{m-1} \sum_{j<1}^{m} \left(\frac{\partial f}{\partial x_i} \right) \left(\frac{\partial f}{\partial x_j} \right) \operatorname{cov}(x_i, x_j) \end{aligned} \tag{10}$$

where m is the number of independent variables; $\frac{\partial f}{\partial x_i}$ and $\frac{\partial f}{\partial x_j}$ are the partial derivatives of the independent variables x_i and x_j, respectively; $\operatorname{var}(x_i)$is the variance of the independent variable x_i; and $\operatorname{cov}(x_i, x_j)$ is the covariance matrix of x_i and x_j.

According to Q. Chen, Laurin, and Valentini (2015), we determined the linear relationship between the standard deviation of the model residuals and $B_{plot,ITA}$. Therefore, the uncertainty of the model residual can be calculated by fitting the standard deviation of the residuals and $B_{plot,\ ITA}$:

$$\sigma_{\varepsilon,\ plot} = \theta \cdot f\left(x, \hat{\beta}\right) \tag{11}$$

where θ is a parameter; $\sigma_{\varepsilon,plot}$ is the standard deviation of the residuals, obtained from the six-step procedure proposed by Hosmer and Lemeshow (1989); and $f\left(x, \hat{\beta}\right)$ is Model III in NSE for AGB estimation.

4. Results

4.1. ITA-based AGB estimation and uncertainty analysis

4.1.1. Individual tree parameters estimation

The U-TLS achieved excellent ITCD accuracy, with the mean r, p, F-scores of 0.81, 0.82, and 0.81, respectively. The 3853 individual trees correctly segmented using U-TLS data were utilized for subsequent individual tree parameter estimation and tree species classification. Figure 5(a) illustrates the accuracy of estimated tree DBH was excellent using the fused point cloud data, which was attributed to the well-detected tree trunks using TLS data. Figure 5(b) depicts the accuracy of estimated tree height, which

was less accurate than that of DBH but still has high accuracy.

4.1.2. Tree species classification

The effectiveness of different data sources and classification algorithms are compared in Table 2. No significant differences were observed between the RF and SVM. Both 1D-CNN and 1D-Resnet50 demonstrated superior performance compared to the aforementioned machine learning models, except when solely using the height or intensity features. The 1D-Resnet50 model achieved the best classification performance (OA: 0.87) based on the combined U-HSIs and U-TLS data.

Figure 6 depicts the confusion matrix for tree species classification based on test samples using 1D-Resnet-50 model and combined U-HSIs and U-TLS data. Korean pine had the highest PA of 0.96; the three hardwood trees and elm had high UA of 0.91 and 0.92, respectively. The UA and PA of Acer mono were 0.72 and 0.75, respectively, lower than those of other tree species. A total of 18 features – 10 LiDAR features and eight hyperspectral features – were chosen using the SHAP value and Resnet50. Supplementary Figure S1 illustrates the contribution of the features to distinguish the seven tree species.

4.1.3. Individual tree AGB estimation

Based on the estimated individual tree parameters and the classified tree species, the individual tree AGB was estimated, and the plot AGB was summed by all tree AGB in sample plot. Figure 7 displays the accuracy assessment results of tree and plot AGB estimates. The accuracy of GB estimation slightly decreased from the tree to the plot level. For high AGB plots, the AGB was underestimated, especially when AGB was greater than 150 Mg/ha. This is because more trees under the canopy tended to go undetected (i.e. omission errors) in plots with large AGB values than in plots with small AGB values in the ITCD procedure. In the individual tree AGB estimates, it is observed that even though the R^2 of the model was high, the RMSE and rRMSE were also high due to the effect of outliers. The most outliers were the high AGB values because the errors of individual tree parameters estimation and tree species classification tended to produce a larger bias for large trees

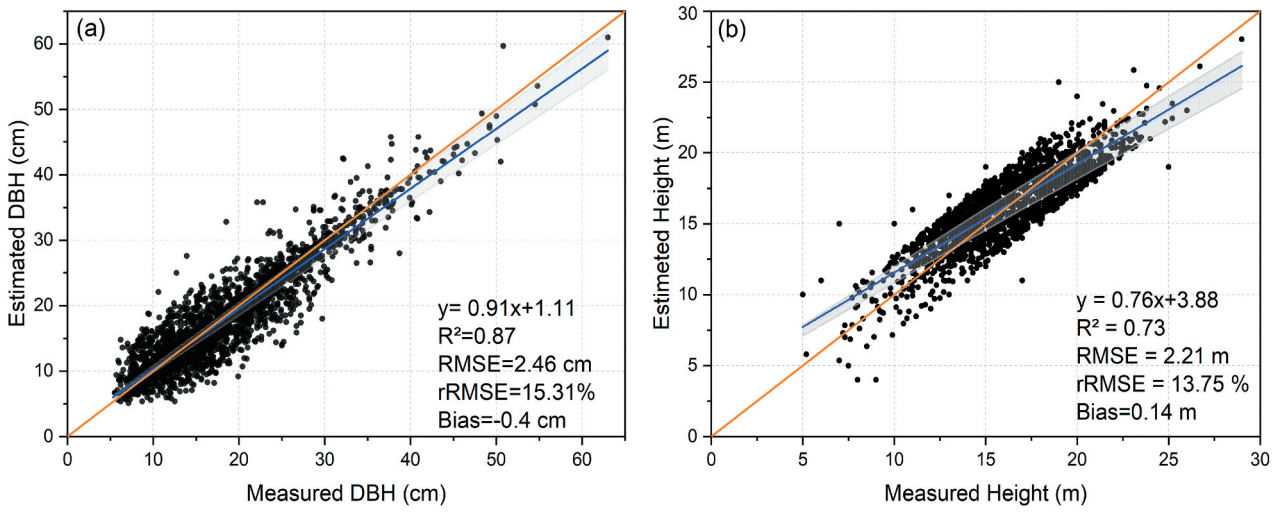

Figure 5. Accuracy assessment of individual tree parameters estimation: (a) DBH; (b) tree height. The orange line is the 1:1 line, and the blue line is the fitted line between the measured and estimated values; the light gray area represents 95% confidence intervals.

Table 2. Overall accuracy of tree species classification using different data sources and models.

		Model			
Data source	Feature	SVM	RF	1D-CNN	1D-Resnet50
U-HSIs	Spectral	0.60	0.61	0.70	0.80
	GLCM	0.61	0.61	0.61	0.82
	Vegetation index	0.62	0.60	0.66	0.76
	All_HSIs	0.63	0.63	0.75	0.82
U-TLS	Height	0.61	0.62	0.53	0.55
	Intensity	0.61	0.60	0.56	0.56
	All_ULS	0.63	0.65	0.74	0.64
U-HSIs+U-TLS	All_HSIs+ULS	0.66	0.65	0.81	0.87

GLCM is the grayscale co-occurrence matrix; All_HSIs is spectral+GLCM+Vegetation index; All_ULS is height+intensity.

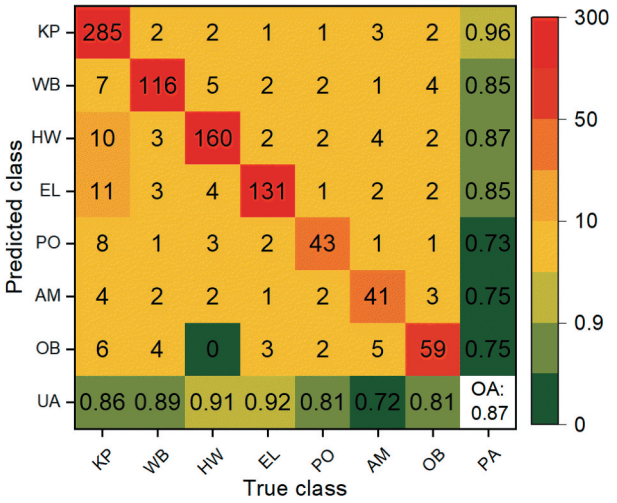

Figure 6. Confusion matrix of the tree species classification using 1D-Resnet-50 model and combined U-HSIs and U-TLS data. Note: KP: Korean pine; WB: white birch; HW: three hardwood trees (including Manchurian ash, Manchurian walnut, and Amur corktree); EL:elm; PO: Populus; AM: acer mono; OB: other broadleaf trees.

than small trees, which increases the model's RMSE and rRMSE.

4.1.4. Uncertainty of tree to plot-level AGB estimation

After 1000 simulations, the plot AGB estimation followed a normal distribution (Figures 8(b,d,f)). Figure 8(e) shows that the total uncertainty of AGB estimation based on ITA was 16.85 Mg/ha, the relative error was 16.29%; Figure 8(f) shows that the mean plot-level AGB simulated value was 103.44 Mg/ha. Although the simulated plot-level AGB values were very close to the three MC simulations, the uncertainty in AGB estimation gradually increased when the individual tree parameter estimation and tree species classification procedures were added to the simulation (from 3.66 Mg/ha in Figure 8(a) to 7.12 Mg/ha in Figure 8(c) to 16.85 Mg/ha in Figure 8(e)).

4.2. Plot- to landscape-level AGB estimation and uncertainty analysis

4.2.1. Extraction of secondary forests

The secondary forests in the study area were extracted using the RF model through the Landsat 8 OLI and ALS data. The OA, PA, and UA of the RF classifier were 0.94, 0.93, and 0.92, respectively.

4.2.2. Plot- to landscape-level AGB estimation

The NSE model for handling $\boldsymbol{x}$ variables with errors was established to connect plot AGB estimates by the ITA with landscape-level AGB. The model fit was satisfactory according to the fitness indices (Table 3) and residual plots (Figure 9). The fitting goodness of DBH (Model II) was better than that of AGB (Model III) and height (Model I).

4.2.3. Uncertainty analysis of plot- to landscape-level AGB estimation

After fitting NSE, model III was used to estimate AGB from the plot to the landscape level. The uncertainty in AGB estimates was mainly caused by uncertainties in the model parameters, independent variables, and model residuals.

The uncertainty of the model parameters was calculated using Equation (9). The uncertainty ($\sigma_{f,\,plot}$) of the AGB model parameters was 5.52 Mg/ha, and the relative uncertainty of $\sigma_{f,\,plot}/\hat{B}_{Plot,\,ITA}$ due to the model parameters was 4.31%.

The uncertainties of the model independent variables were mainly caused by the estimation error of H_{ALS} and DBH_{ITA} in models I and II of NSE.

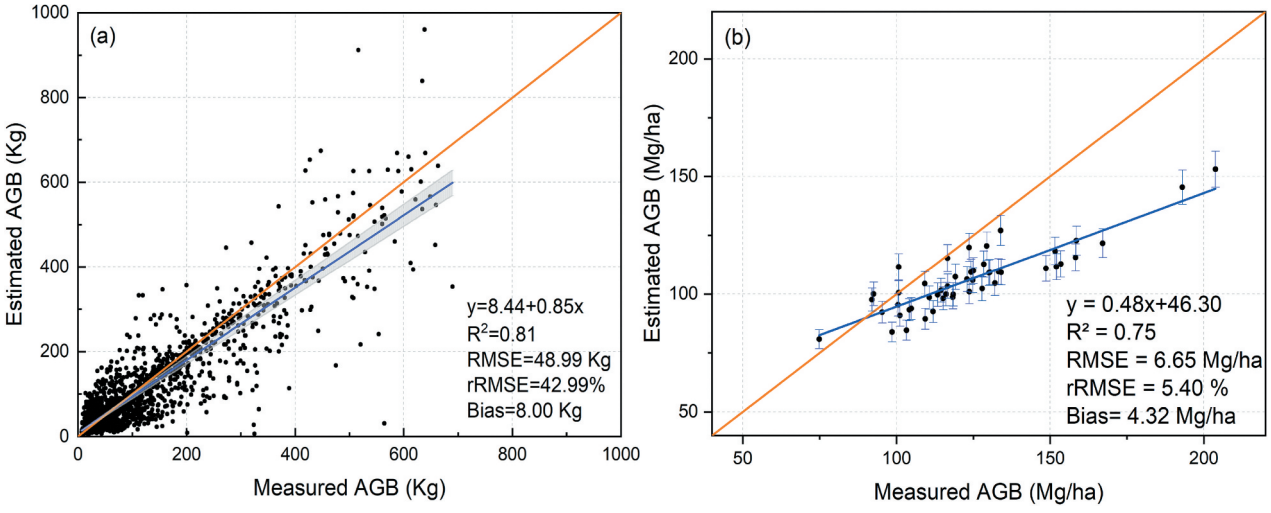

Figure 7. Accuracy assessment of (a) individual tree AGB estimates; (b) plot AGB estimates. The orange line is the 1:1 line, and the blue line is the fitted line between the measured and estimated values. The light gray area represents 95% confidence intervals and the vertical lines are error bars.

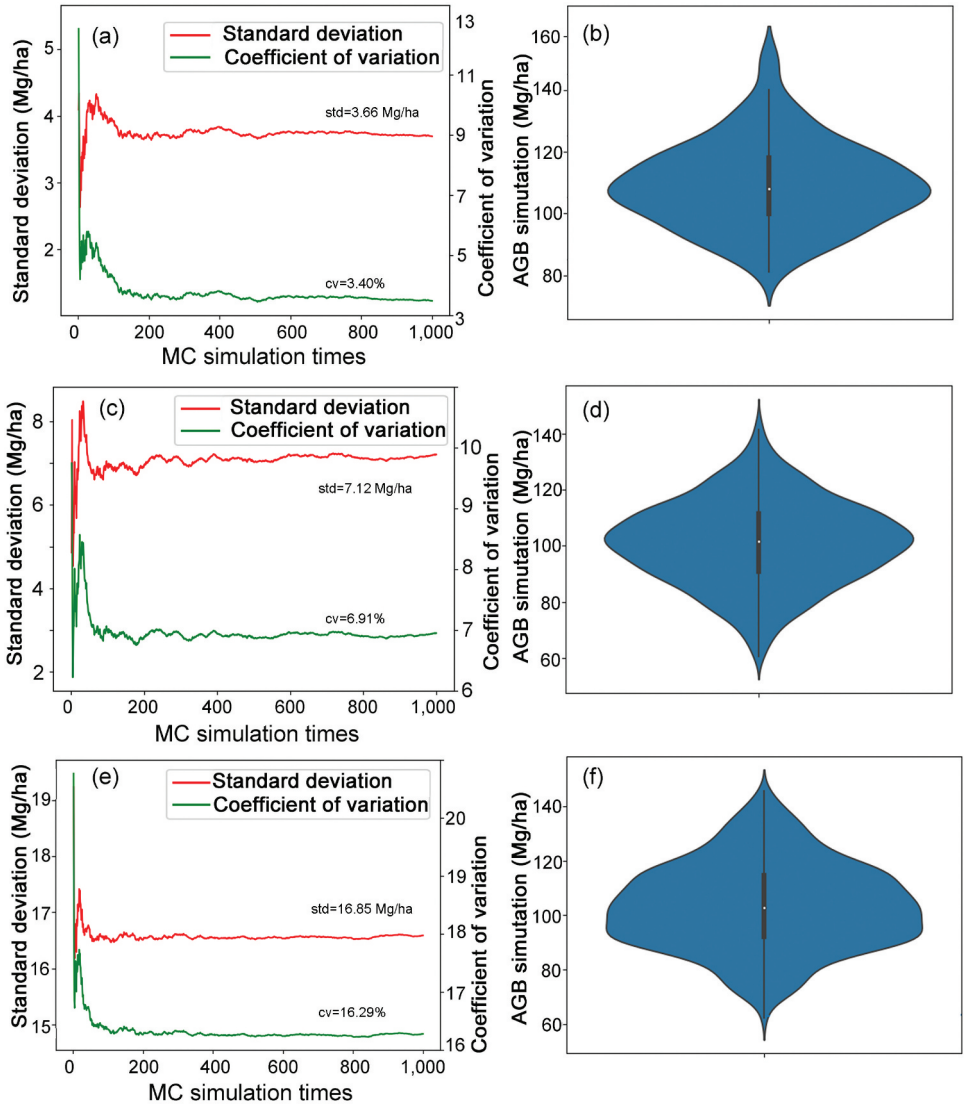

Figure 8. Uncertainty and AGB simulation in ITCD, individual tree parameter estimation, and tree species classification after 1000 MC simulations. (a) and (b) represent the uncertainty induced from ITCD procedure and the simulated plot-level AGB in the violin plot, respectively; (c) and (d) represent the uncertainty induced from ITCD and individual tree parameter estimation procedures and the simulated plot-level AGB in the violin plot, respectively; and (e) and (f) represent the uncertainty induced from ITCD, individual tree parameter estimation and tree species classification procedures and the simulated plot-level AGB in the violin plot, respectively.

Table 3. Parameters estimates and model fitting of the NSE.

Model	a_i	b_i	c_i	R^2	RMSE	rRMSE (%)
NSE (Model I)	−0.15	0.46	0.19	0.64	1.05 m	8.75
NSE (Model II)	−2.71	0.70	-	0.72	1.12 cm	8.00
NSE (Model III)	32.09	0.27	0.26	0.69	9.91 Mg/ha	10.43

NSE is nonlinear simultaneous equation and i = [1,2,3] denote the fitted parameters of the model I, model II and model III in NSE, respectively.

According to Equation (10), variance of the independent variables ($VAR(DBH_{ITA})$ and $VAR(H_{ALS})$) were 2.62 and 13.10, respectively. The uncertainty due to the model independent variables ($\sigma_{x,\ plot}$) was 14.56 Mg/ha, with a relative uncertainty ($\sigma_{x,\ plot}/\hat{B}_{Plot,\ ITA}$) of 11.39%.

The residual uncertainty of the AGB estimation model can be calculated using Equation (11). The estimation results are shown in Equation (12). This implies that the relative uncertainty ($\sigma_{\varepsilon,\ plot}/\hat{B}_{Plot,\ ITA}$) due to the model residuals at the plot level was 19.75% and its uncertainty ($\sigma_{\varepsilon,plot}$) was 25.25 Mg/ha.

$$\sigma_{\varepsilon,\ plot} = 0.1975\hat{B}_{Plot,\ ITA} \tag{12}$$

Based on Equation (8), the total uncertainty of AGB estimation was 29.66 Mg/ha and the relative uncertainty ($\sigma_{t,\ plot}/\hat{B}_{Plot,\ ITA}$) was 23.20%. Figure 10 shows that among the three uncertainties for the NSE-based AGB estimation, the uncertainty related to the model residuals

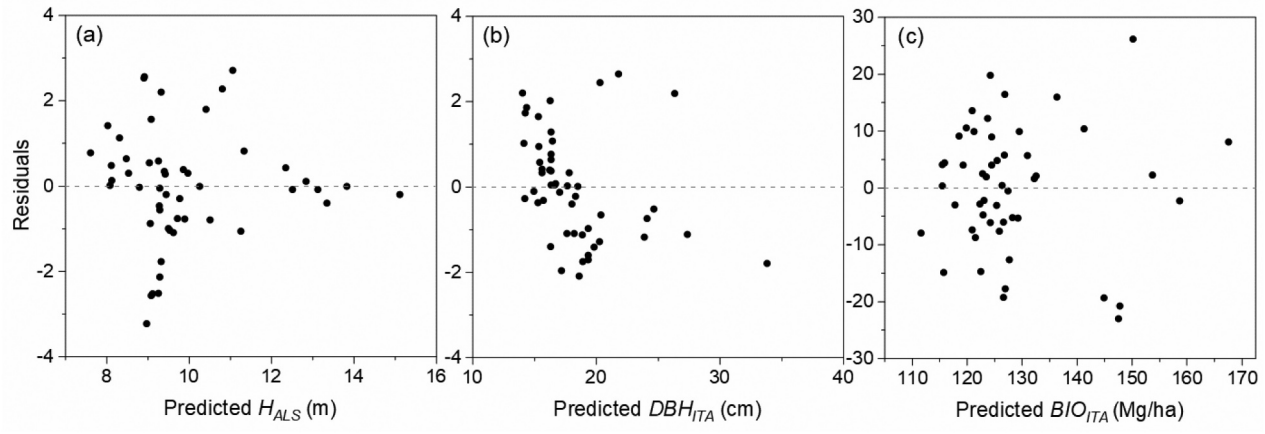

Figure 9. Residuals plots of (a) model I; (b) model II; and (c) model III in the NSE.

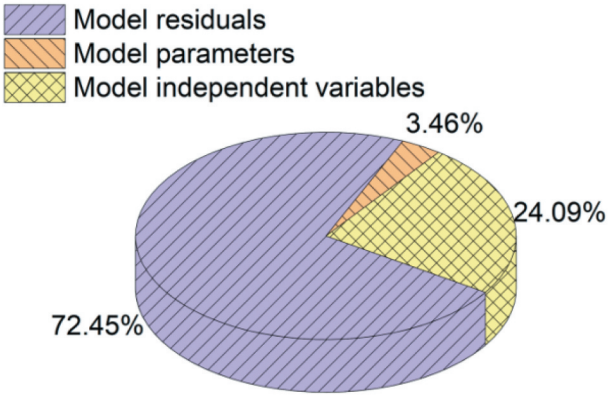

Figure 10. Model residuals, parameters and independent variable uncertainties as a proportion of total uncertainty.

is the largest (72.45%), followed by the model independent variables (24.09%) and model parameters (3.46%).

4.3. Mapping landscape-level AGB and its uncertainty

The landscape-level AGB estimates and uncertainty of secondary forests at Maoershan Forest Farm are displayed in Figure 11. The spatial distributions of the uncertainties of the model residuals and model independent variables were consistent, and the uncertainty was significantly higher than that of the model parameters. The total uncertainty was between 20 and 80 Mg/ha (Figure 11(d)). The range of AGB estimates was 20–220 Mg/ha (Figure 11(e)), and the mean value of AGB estimates was 99.08 Mg/ha. It can be seen that areas with high uncertainty in AGB estimation usually have large AGB values.

5. Discussions

5.1. Individual tree-based AGB estimation and its uncertainty analysis

Under the ITA framework, ITCD, individual tree parameter estimation and tree species classification are critical for accurate AGB estimation. A reliable ITCD serves as the foundation for estimating AGB. Many low trees that are shadowed by taller trees can be difficult to distinguish from ALS or ULS data in dense forests, particularly in secondary forests (Zhao et al. 2017; Zhen, Quackenbush, and Zhang 2014). The ITCD accuracy in this study (average F-score: 0.81) was higher than that in previous studies (Zhao et al. 2022; Zhen et al. 2022) thanks to the fused U-TLS data. Compared to ULS and TLS, the fused U-TLS clearly scans the complete trunk and canopy, enabling more accurate seed point generation and canopy boundary delineation during the ITCD process. U-TLS can also improve the accuracy of parameter estimation. The application of TLS data alone caused an underestimation of individual tree heights, whereas ULS data led to a favorable estimation of tree heights according to (Y. Zhao et al. 2023). Moreover, it is hard to scan complete trunk information from the ULS data in forests with high canopy closure, individual tree DBH cannot be directly estimated and is usually inverted using the height-DBH model (Moe et al. 2020; Zhao et al. 2022). The accuracy of DBH estimation was greatly improved by merging the ULS and TLS data, which considerably reduced the error caused by the height-DBH model. The small uncertainties associated with ITCD and individual tree parameter estimation can be attributed to the combined effect of multiple near-surface LiDAR data, which enables adequate detection of low individual tree within the plot.

This study introduced errors in tree species classification into the ITA-based AGB estimation so that the uncertainty in AGB estimation for complex mixed forests could be quantified, rather than being limited to pure forests. 1D-Resnet50 performed best when combined with point cloud and hyperspectral features. This suggests that the deep CNN algorithm is effective for tree species classification with combined hyperspectral and LiDAR data because of the algorithm's ability to adequately extract abstract features through deep convolutional networks (Pouyanfar et al. 2019).

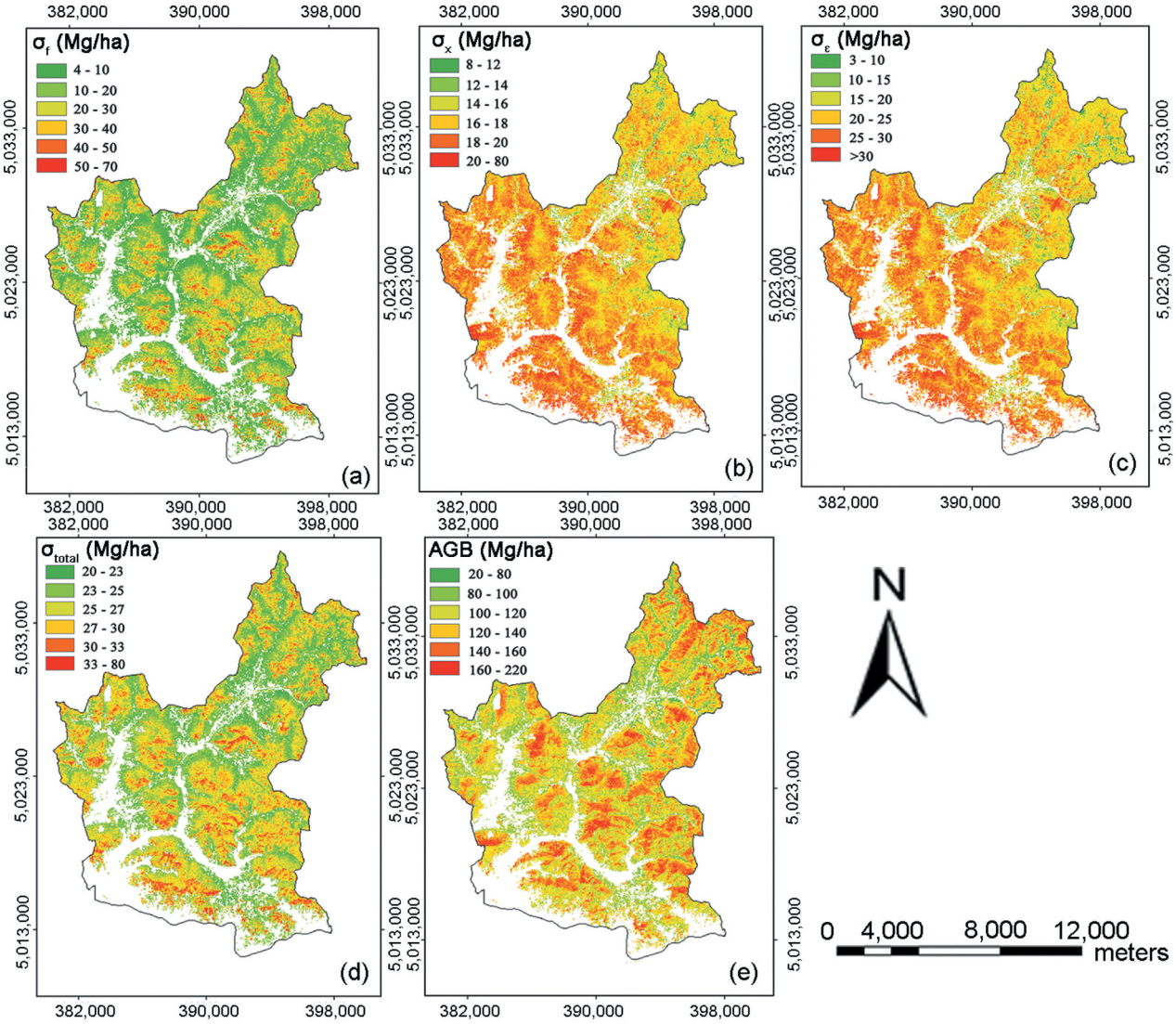

Figure 11. Spatial distribution of landscape-level AGB estimates of secondary forests and uncertainties based on error propagation principle. (a)-(e) represent the uncertainties of the model parameters, the model independent variables, the model residuals, the total uncertainty, and the landscape-level AGB estimates of secondary forests, respectively.

This agrees with the findings of a previous research on DL algorithms for tree species classification (Mäyrä et al. 2021). Furthermore, a 3D CNN is a good choice for modeling high-dimensional data as it can handle both texture and spectral information, which is a great advantage for tree species classification (Zhang et al. 2023). Although the accuracy of tree species classification in this study was high (OA: 0.85), the uncertainty of tree species classification was greater than that in ITCD and individual tree parameter estimation (Figure 8) due to the use of the allometric growth equation with incorrect tree species. In a subsequent study, work should be done to enhance the accuracy of AGB estimates by modeling individual tree AGB directly without tree species classification.

This study aims to investigate the uncertainty of AGB estimation using remote sensing techniques, we assumed that the biomass additive equations were error-free; therefore, the final uncertainty was underestimated because of errors in the biomass additive equations. The employed biomass additive equations in this study demonstrated a high level of accuracy (Dong, Li, and Song 2015; Dong, Zhang, and Li 2015) and the underestimation was minimal. This partially explains why the uncertainty in the plot AGB estimates was much lower in this study (CV: 16.29%) than in previous studies based on ALS-based allometric growth equations with CV of 214% (Xu et al. 2018) and 58–66% (Chave et al. 2004; Chen, Laurin, and Valentini 2015). This indicates that it is critical to apply accurate allometric growth equations obtained from the harvesting method to calculate the reference AGB and reduce the error in estimating AGB from remote sensing data. In addition, benefiting from the combined employment of multiple near-surface remote sensing data, omission and commission errors in ITCD (r: 0.81; p: 0.82) and errors of individual tree parameter estimation (rRMSE: 15.31% of DBH; 13.75% of tree height) were low, which greatly reduced the uncertainty in the tree to plot-level AGB estimation.

5.2. Plot- to landscape-level AGB estimation and uncertainty analysis

Because NSE can handle inputs with errors in the independent variables, it is a good approach to support the use of variables estimated using remote sensing data to invert AGB/carbon stocks. Furthermore, AGB estimation at multi-levels (individual trees, plots and landscape) achieved good results, even for mixed secondary forests with complex structures. The AGB estimation errors obtained in this study (RMSE: 9.91 Mg/ha, rRMSE: 10.43%) were much lower than the requirements of satellite remote sensing missions (error less than 20 Mg/ha or 20%) according to the assertions of previous studies (Hall et al. 2011; Zolkos, Goetz, and Dubayah 2013). Our result using ITA-based approach in terms of rRMSE at plot level were better (rRMSE = 10.43%, NSE (Model III)) than the values reported using ABA-approach (27.22% −51.63%) for AGB estimates in Guerra-Hernández et al. (2022) at the regional level in Spain.

This study demonstrates a significantly improved accuracy, thereby contributing to the employment of refined algorithms and high-resolution data sources. Among the three uncertainties in the NSE-based AGB estimation, the largest was the uncertainty of model residuals, followed by the uncertainties of model independent variables and model parameters. This was similar to the results of previous studies but with some differences. For example, Chen, Laurin, and Valentini (2015) employed ALS to develop a generalized linear model to estimate AGB at the pixel scale and found that the relative uncertainties associated with model residuals, parameters, and independent variables were 47.9%, 16.2%, and 16.0% (80.5%, 10.6%, and 8.8% of the total uncertainty, respectively). The uncertainty caused by the model residuals was the largest, as observed in the present study. Additionally, the uncertainty of model independent variables had a larger share. This was primarily because the independent variables in the present study (DBH_{ITA} and H_{ALS}) were estimated using individual tree detection techniques, while in other studies, the error of the independent variables (LiDAR-based variables) was assumed to be 10% (Chen, Laurin, and Valentini 2015) or 5% (Asner et al. 2012). Our model parameter uncertainties (3.46%) were slightly better than relative uncertainties associated with model parameter in Guerra-Hernández et al. (2022) who reported a relative standard error for regional level forest type-specific ALS-based estimates of AGB from 3.63% to 12.58%, although they did not consider the source of uncertainty for vegetation strata classification.

The model accuracies of NSE were slightly higher than those of seemingly unrelated regression (Table 3 vs. Supplementary Table S9), which is a multiple-equation regression model for multiple correlated but not perfectly correlated dependent variables, indicating that NSE was very effective in handling models with errors in the independent variables. This outcome is comparable to the study of Fu et al. (2016) that examined these two models. Large-scale (e.g. national, regional scale) forest AGB estimation and statistics are the basis of global carbon cycle, climate change research, and an important indicator to quantify the quality of forest growth. Compared to previous forest AGB maps (Su et al. 2016; Zhang, Liang, and Sun 2014), the AGB estimates in this study (mean AGB: 99.08 Mg/ha; RMSE: 9.91 Mg/ha) were higher. For example, Zhang, Liang, and Sun (2014) reported that the average forest AGB was 83.50 Mg/ha (RMSE: 26.76 Mg/ha) in northeast China; and Su et al. (2016) estimated the average forest AGB to be 92.79 Mg/ha (RMSE: 26.08 Mg/ha) in temperate conifer-broadleaf mixed forests. Previous investigations relied primarily on ABA-based AGB estimation, such as those derived from Landsat imagery, whereas this study focused on individual-tree measurements. This latter approach provides a finer spatial resolution, allowing for a more detailed analysis of the spatial characteristics and structural attributes of the trees.

5.3. Limitations and future research

Despite quantifying multiple error sources, some errors were not considered in AGB estimation, such as sampling error, attribute measurement error, and tree positioning error. Attribute measurement and tree positioning errors are typically considered systematic errors and are generally small in magnitude (Berger et al. 2014; Chen, Laurin, and Valentini 2015). On the other hand, sampling error can be substantial, as they are influenced by the sampling method, sample size, and representativeness of the sample. Sampling errors can be assessed by Monte Carlo combined with Taylor series expansion methods (Fu et al. 2017). In addition, there exist matching errors between the sample plot and the image pixel generated by ground positioning, image georeferencing, and inconsistent sizes of plots and image pixels (Wang et al. 2009). To enhance the accuracy of AGB estimation, it is recommended to quantify these errors in the future. Although this study conducted the multi-scale AGB estimation for complex secondary forests, the performance of the framework should be tested in other mixed forests in the future to demonstrate its generalization and transferability. Integrating the MC simulation process into a Python library would be a meaningful work, so that the methodology of this study can be applied in other areas. TLS devices are too bulky and difficult for surveyors to use in forested areas with many shrubs. With the advent of mobile LiDAR (e.g. handheld and backpack LiDAR), it can

provide good estimation of forest parameters (Xu et al. 2021). If mobile LiDAR can achieve similar accuracy of DBH estimation as TLS, it will become a very convenient and promising tool for individual tree-based AGB estimation (Liang et al. 2024). In addition, NSE requires independent homogeneous distributions but does not account for potential autocorrelation of trees; NSE can be improved to accommodate autocorrelation of trees in future studies.

6. Conclusions

The main contributions of this study were proposing a framework to assess the performance of AGB estimation of secondary forests from the tree to landscape level and analyzing the uncertainties induced by different procedures, including ITCD, individual tree parameter estimation, tree species classification, model residuals, model parameters, and model independent variables of NSE. The plot-level AGB estimates achieved a satisfactory accuracy using a variety of near-ground remote sensing data. For the ITA-based AGB estimation, the uncertainty of ITCD was 3.66 Mg/ha, which increased to 7.12 Mg/ha when individual tree parameter estimation was involved. The final uncertainty reached 16.85 Mg/ha, and the simulated mean AGB was 103.44 Mg/ha using MC simulations. NSE was used to upscale AGB estimation from the plot to the landscape level using ALS (R^2: 0.69; RMSE: 9.91 Mg/ha; rRMSE: 10.43%). The uncertainties of model parameters, independent variables, and residuals were 5.52 Mg/ha, 14.56 Mg/ha, and 25.25 Mg/ha, respectively, based on the error propagation principle.

This study highlighted the uncertainty at various levels in the remote sensing-based AGB estimation process. The application of NSE is a good solution to the problem of independent variable errors caused by variables estimated by remote sensing data in modeling. The proposed framework can provide technical support for AGB estimation and uncertainty analysis from individual trees to plot the landscape level for secondary forests or other mixed forests in other areas. This framework can be useful not only for large-scale remote sensing mapping but also for fine plot-level studies based on individual trees. This study would provide a foundation for precise forestry, sustainable forest management, and carbon neutrality.

Disclosure statement

No potential conflict of interest was reported by the author(s).

Funding

This work is supported by the Key Project of the China National Key Research and Development Program [grant number 2021YFD2200401], the National Natural Science Foundation of China [grant number 32071677], the National Forestry and Grassland Data Center-Heilongjiang platform [grant number 2005DKA32200-OH], and Korea Environment Industry & Technology Institute (KEITI) through Project for developing an observation-based GHG emissions geospatial information map, funded by Korea Ministry of Environment (MOE) [grant number RS-2023-00232066].

Notes on contributors

Ye Ma a graduate of Northeast Forestry University, obtained his Ph.D. He is currently employed at the School of Geographic Sciences, Harbin Normal University. He is engaged in the research of forest remote sensing, deep learning and forest carbon storage estimation and has published seven papers. His current research interest includes forestry remote sensing and GIS, temporal and spatial statistics, and artificial intelligence based on spatial data.

Jungho Im is a professor of the Department Urban and Environmental Engineering, Ulsan National Institute of Science and Technology. He received his Ph.D. degree from the University of South Carolina in 2006. He has published more than 120 papers. His current research interest includes remote sensing applications, spatial analysis, earth observation, hyperspectral image analysis, geospatial science, and water color remote sensing.

Zhen Zhen is an associate professor of the Department of Forest Management, School of Forestry, Northeast Forestry University (NEFU). She received her Ph.D. degree from the State of New York College of Environmental Science and Forestry (SUNY-ESF) in 2013. She also obtained a concurrent MPS degree in Geospatial Information Science and Engineering at SUNY-ESF. She has published more than 40 papers, one academic monograph, and two textbooks. Since 2013, she has managed nine projects as a PI and participated in several projects as a backbone member. Her current research interest includes forestry remote sensing and GIS, temporal and spatial statistics, and artificial intelligence based on spatial data.

Yinghui Zhao is a professor of the Department of Forest Management, School of Forestry, Northeast Forestry University (NEFU). She received her MS and Ph.D. degrees in forest management at NEFU. She was a visiting scholar of the State University of New York College of Environmental Science and Forestry (SUNY-ESF) from October 2017 to October 2018. She has also published more than 40 papers, one textbook. She has managed 13 projects as a PI and participated in more than 10 projects. She won three scientific research awards and seven teaching quality awards. Her current research interest includes forestry remote sensing and GIS and digital forestry.

ORCID

Ye Ma http://orcid.org/0000-0002-6476-6967
Jungho Im http://orcid.org/0000-0002-4506-6877
Zhen Zhen http://orcid.org/0000-0001-9281-4260
Yinghui Zhao http://orcid.org/0000-0002-1933-8357

Data availability statement

The data that support the findings of this study are available on request from the corresponding author (Z.Z). The data are not publicly available because it contains information that could compromise the privacy of research participants.

References

Almeida, C. T. D., L. S. Galvão, L. Aragão, J. P. Ometto, A. D. Jacon, F. R. Pereira, L. Y. Sato, et al. 2019. "Combining LiDAR and Hyperspectral Data for Aboveground Biomass Modeling in the Brazilian Amazon Using Different Regression Algorithms." *Remote Sensing of Environment* 232:111323. https://doi.org/10.1016/j.rse.2019.111323.

Amini, S., S. Homayouni, A. Safari, and A. Darvishsefat. 2018. "Object-Based Classification of Hyperspectral Data Using Random Forest Algorithm." *Geo-Spatial Information Science* 21 (2): 127–138. https://doi.org/10.1080/10095020.2017.1399674.

Asner, G. P., J. K. Clark, J. Mascaro, G. A. García, K. D. Chadwick, D. A. Encinales, G. Paez-Acosta, et al. 2012. "High-Resolution Mapping of Forest Carbon Stocks in the Colombian Amazon." *Biogeosciences* 9 (7): 2683–2696. https://doi.org/10.5194/bg-9-2683-2012.

Berger, A., T. Gschwantner, R. E. McRoberts, and K. Schadauer. 2014. "Effects of Measurement Errors on Individual Tree Stem Volume Estimates for the Austrian National Forest Inventory." *Forest Science* 60 (1): 14–24. https://doi.org/10.5849/forsci.12-164.

Bergstra, J., and Y. Bengio. 2012. "Random Search for Hyper-Parameter Optimization." *Journal of Machine Learning Research* 13 (1): 281–305.

Besl, P. J., and N. D. McKay. 1992. "A Method for Registration of 3-D Shapes." *IEEE Transactions on Pattern Analysis and Machine Intellligence* 14 (2): 239–256. https://doi.org/10.1109/34.121791.

Brede, B., L. Terryn, N. Barbier, H. M. Bartholomeus, R. Bartolo, K. Calders, G. Derroire, et al. 2022. "Non-Destructive Estimation of Individual Tree Biomass: Allometric Models, Terrestrial and UAV Laser Scanning." *Remote Sensing of Environment* 280:113180. https://doi.org/10.1016/j.rse.2022.113180.

Brovkina, O., E. Cienciala, P. Surový, and P. Janata. 2018. "Unmanned Aerial Vehicles (UAV) for Assessment of Qualitative Classification of Norway Spruce in Temperate Forest Stands." *Geo-Spatial Information Science* 21 (1): 12–20. https://doi.org/10.1080/10095020.2017.1416994.

Chave, J., C. Richard, A. Salomon, H. Andres, L. Suzanne, and P. Rolando. 2004. "Error Propagation and Scaling for Tropical Forest Biomass Estimates." *Philosophical Transactions of the Royal Society of London Series B: Biological Sciences* 359 (1443): 409–420. https://doi.org/10.1098/rstb.2003.1425.

Chen, J., X. Li, Z. Huang, J. Xuan, C. Chen, M. Hu, C. Tan, et al. 2024. "Forest Age Estimation Using UAV-LiDAR and Sentinel-2 Data with Machine Learning Algorithms-a Case Study of Masson Pine (*Pinus Massoniana*)." *Geo-Spatial Information Science* (June): 1–21. https://doi.org/10.1080/10095020.2024.2362752.

Chen, Q., G. V. Laurin, and R. Valentini. 2015. "Uncertainty of Remotely Sensed Aboveground Biomass Over an African Tropical Forest: Propagating Errors from Trees to Plots to Pixels." *Remote Sensing of Environment* 160:134–143. https://doi.org/10.1016/j.rse.2015.01.009.

Cheng, K., and J. Wang. 2019. "Forest Type Classification Based on Integrated Spectral-Spatial-Temporal Features and Random Forest Algorithm—A Case Study in the Qinling Mountains." *Forests* 10 (7): 559. https://doi.org/10.3390/f10070559.

Diamantidis, N. A., D. Karlis, and E. A. Giakoumakis. 2000. "Unsupervised Stratification of Cross-Validation for Accuracy Estimation." *Artificial Intelligence* 116:1–16. https://doi.org/10.1016/S0004-3702(99)00094-6.

Dong, L. H., F. R. Li, and Y. W. Song. 2015. "Error Structure and Additivity of Individual Tree Biomass Model for Four Natural Conifer Species in Northeast China." *Chinese Journal of Applied Ecology* 26 (3): 704–714. https://doi.org/10.13287/j.1001-9332.20150106.011.

Dong, L. H., L. J. Zhang, and F. R. Li. 2015. "Developing Additive Systems of Biomass Equations for Nine Hardwood Species in Northeast China." *Trees* 29 (4): 1149–1163. https://doi.org/10.1007/s00468-015-1196-1.

Du, C. Y., W. Y. Fan, Y. Ma, H. Jin, and Z. Zhen. 2021. "The Effect of Synergistic Approaches of Features and Ensemble Learning Algorithms on Aboveground Biomass Estimation of Natural Secondary Forests Based on ALS and Landsat 8." *Sensors (Switzerland)* 21 (17): 5974. https://doi.org/10.3390/s21175974.

Fu, L. Y., Y. Lei, G. Wang, H. Bi, S. Tang, and X. Song. 2016. "Comparison of Seemingly Unrelated Regressions with Error-In-Variable Models for Developing a System of Nonlinear Additive Biomass Equations." *Trees* 30 (3): 839–857. https://doi.org/10.1007/s00468-015-1325-x.

Fu, L. Y., Y. Lei, W. Zeng, R. Hao, G. Zhang, Q. Zhong, and M. Xu. 2017. "Uncertainty Assessment in Aboveground Biomass Estimation at the Regional Scale Using a New Method Considering Both Sampling Error and Model Error." *Canadian Journal of Forest Research* 47 (8): 1095–1103. https://doi.org/10.1139/cjfr-2016-0436.

Gander, W., G. H. Golub, and R. Strebel. 1994. "Least-Squares Fitting of Circles and Ellipses." *BIT Numerical Mathematics* 34 (4): 558–578. https://doi.org/10.1007/BF01934268.

Gertner, G., X. Cao, and H. Zhu. 1995. "A Quality Assessment of a Weibull Based Growth Projection System." *Forest Ecology & Management* 71 (3): 235–250. https://doi.org/10.1016/0378-1127(94)06104-Q.

Gertner, G., P. Parysow, and B. Guan. 1996. "Projection Variance Partitioning of a Conceptual Forest Growth Model with Orthogonal Polynomials." *Forest Science* 42 (4): 474–486. https://doi.org/10.1093/forestscience/42.4.474.

Goldbergs, G., S. R. Levick, M. Lawes, and A. Edwards. 2018. "Hierarchical Integration of Individual Tree and Area-Based Approaches for Savanna Biomass Uncertainty Estimation from Airborne LiDAR." *Remote Sensing of Environment* 205:141–150. https://doi.org/10.1016/j.rse.2017.11.010.

Guerra-Hernández, J., B. Botequim, S. Bujan, A. Jurado-Varela, J. A. Molina-Valero, A. Martínez-Calvo, and C. Pérez-Cruzado. 2022. "Interpreting the Uncertainty of Model-Based and Design-Based Estimation in Downscaling Estimates from NFI Data: A Case-Study in Extremadura (Spain." *GIScience & Remote Sensing* 59:686–704. https://doi.org/10.1080/15481603.2022.2051383.

Hall, F. G., K. Bergen, J. B. Blair, R. Dubayah, R. Houghton, G. Hurtt, J. Kellndorfer, et al. 2011. "Characterizing 3D Vegetation Structure from Space: Mission Requirements."

Remote Sensing of Environment 115 (11): 2753–2775. https://doi.org/10.1016/j.rse.2011.01.024.

Hartlinga, S., V. Sagan, and M. Maimaitijiang. 2021. "Urban Tree Species Classification Using UAV-Based Multi-Sensor Data Fusion and Machine Learning." *GIScience & Remote Sensing* 58 (8): 1250–1275. https://doi.org/10.1080/15481603.2021.1974275.

He, K., X. Zhang, S. Ren, and J. Sun. 2016. "Deep Residual Learning for Image Recognition." *IEEE Conference on Computer Vision and Pattern Recognition*, 770–778. https://doi.org/10.1109/CVPR.2016.90.

Hosmer, D., and S. Lemeshow. 1989. *Applied Logistic Regression*. New York: John Wiley & Sons.

Huo, L., E. Lindberg, and J. Holmgren. 2022. "Towards Low Vegetation Identification: A New Method for Tree Crown Segmentation from LiDAR Data Based on a Symmetrical Structure Detection Algorithm (SSD)." *Remote Sensing of Environment* 270:112857. https://doi.org/10.1016/j.rse.2021.112857.

Ji, Y., F. Zhang, W. Zhang, L. Zhao, K. Xu, J. Shi, G. Huang, Q. Jing, L. Wang, and F. Yang. 2024. "Exploring Optimal Combinations of Multi-Frequency Polarimetric SAR Observations to Estimate Forest Above-Ground Biomass." *Geo-Spatial Information Science* (February): 1–19. https://doi.org/10.1080/10095020.2024.2311867.

Jin, H., Y. Zhao, U. Pak, Z. Zhen, and K. So. 2024. "Assessing the Effect of Ensemble Learning Algorithms and Validation Approach on Estimating Forest Aboveground Biomass: A Case Study of Natural Secondary Forest in Northeast China." *Geo-Spatial Information Science* (February): 1–20. https://doi.org/10.1080/10095020.2024.2311261.

Kaartinen, H., J. Hyyppä, X. Yu, M. Vastaranta, H. Hyyppä, A. Kukko, M. Holopainen, et al. 2012. "An International Comparison of Individual Tree Detection and Extraction Using Airborne Laser Scanning." *Remote Sensing* 4 (4): 950–974. https://doi.org/10.3390/rs4040950.

Li, W., Q. Guo, M. K. Jakubowski, and M. Kelly. 2012. "A New Method for Segmenting Individual Trees from the Lidar Point Cloud." *Photogrammetric Engineering & Remote Sensing* 78 (1): 75–84. https://doi.org/10.14358/PERS.78.1.75.

Liang, X., H. Yao, H. Qi, and X. Wang. 2024. "Forest in situ Observations Through a Fully Automated Under-Canopy Unmanned Aerial Vehicle." *Geo-Spatial Information Science* 27 (4): 983–999. https://doi.org/10.1080/10095020.2024.2322765.

Liu, K., X. Shen, L. Cao, G. Wang, and F. Cao. 2018. "Estimating Forest Structural Attributes Using UAV-LiDAR Data in Ginkgo Plantations." *ISPRS Journal of Photogrammetry & Remote Sensing* 146:465–482. https://doi.org/10.1016/j.isprsjprs.2018.11.001.

Matasci, G., T. Hermosilla, M. A. Wulder, J. C. White, N. C. Coops, G. W. Hobart, and H. S. J. Zald. 2018. "Large-Area Mapping of Canadian Boreal Forest Cover, Height, Biomass and Other Structural Attributes Using Landsat Composites and Lidar Plots." *Remote Sensing of Environment* 209:90–106. https://doi.org/10.1016/j.rse.2017.12.020.

Mäyrä, J., S. Keski-Saari, S. Kivinen, T. Tanhuanpää, P. Hurskainen, P. Kullberg, L. Poikolainen, et al. 2021. "Tree Species Classification from Airborne Hyperspectral and LiDAR Data Using 3D Convolutional Neural Networks." *Remote Sensing of Environment* 256:112322. https://doi.org/10.1016/j.rse.2021.112322.

Merrin, J. 2017. *Introduction to Error Analysis: The Science of Measurements, Uncertainties, and Data Analysis*. Charleston: CreateSpace Independent Publishing Platform.

Moe, K., T. Owari, N. Furuya, and T. Hiroshima. 2020. "Comparing Individual Tree Height Information Derived from Field Surveys, LiDAR and UAV-DAP for High-Value Timber Species in Northern Japan." *Forests* 11 (2): 223. https://doi.org/10.3390/f11020223.

Molnar, C. 2020. *Interpretable Machine Learning: A Guide for Making Black Box Models Explainable*. Morrisville: Lulu Press.

Mountrakis, G., J. Im, and C. Ogole. 2011. "Support Vector Machines in Remote Sensing: A Review." *ISPRS Journal of Photogrammetry & Remote Sensing* 66 (3): 247–259. https://doi.org/10.1016/j.isprsjprs.2010.11.001.

Navarro, A., M. Young, B. Allan, P. Carnell, P. Macreadie, and D. Ierodiaconou. 2020. "The Application of Unmanned Aerial Vehicles (UAVs) to Estimate Above-Ground Biomass of Mangrove Ecosystems." *Remote Sensing of Environment* 242:111747. https://doi.org/10.1016/j.rse.2020.111747.

Patel, N., and A. Majumdar. 2011. "Comparative Assessment of the Relationship of Satellite Data with the Above Ground Biomass of Sal Trees (Shorea Robusta) Determined from Phenologically Different Time Periods." *Geo-Spatial Information Science* 14 (3): 177–183. https://doi.org/10.1007/s11806-011-0492-1.

Peng, S., N. He, G. Yu, and Q. Wang. 2017. "Aboveground Biomass Estimation at Different Scales for Subtropical Forests in China." *Botanical Studies* 58 (1): 45. https://doi.org/10.1186/s40529-017-0199-1.

Persson, H. J., M. Ekström, and G. Ståhl. 2022. "Quantify and Account for Field Reference Errors in Forest Remote Sensing Studies." *Remote Sensing of Environment* 283:113302. https://doi.org/10.1016/j.rse.2022.113302.

Pouyanfar, S., S. Sadiq, Y. Yan, H. Tian, Y. Tao, M. Reyes, M. Shyu, S. Chen, and S. S. Iyengar. 2019. "A Survey on Deep Learning: Algorithms, Techniques, and Applications." *ACM Computing Surveys* 51 (5): 1–36. https://doi.org/10.1145/3234150.

Qin, H., W. Zhou, Y. Yao, and W. Wang. 2022. "Individual Tree Segmentation and Tree Species Classification in Subtropical Broadleaf Forests Using UAV-Based LiDAR, Hyperspectral, and Ultrahigh-Resolution RGB Data." *Remote Sensing of Environment* 280:113143. https://doi.org/10.1016/j.rse.2022.113143.

Qiu, P. H., D. Wang, X. Zou, X. Yang, G. Xie, S. Xu, and Z. Zhong. 2019. "Finer Resolution Estimation and Mapping of Mangrove Biomass Using UAV LiDAR and WorldView-2 Data." *Forests* 10 (10): 871. https://doi.org/10.3390/f10100871.

Quan, Y., M. Li, Y. Hao, J. Liu, and B. Wang. 2023. "Tree Species Classification in a Typical Natural Secondary Forest Using UAV-Borne LiDAR and Hyperspectral Data." *GIScience & Remote Sensing* 60 (1): 2171706. https://doi.org/10.1080/15481603.2023.2171706.

Raychaudhuri, S. 2008. "Introduction to Monte Carlo Simulation." *IEEE Winter simulation conference*, 91–100. https://doi.org/10.1109/WSC.2008.4736059.

Rödig, E., N. Knapp, R. Fischer, F. Bohn, R. Dubayah, H. Tang, and A. Huth. 2019. "From Small-Scale Forest Structure to Amazon-Wide Carbon Estimates." *Nature Communications* 10 (1): 5088. https://doi.org/10.1038/s41467-019-13063-y.

Sothe, C., C. M. De Almeida, M. B. Schimalski, L. E. C. La Rosa, J. D. B. Castro, R. Q. Feitosa, M. Dalponte, et al.

2020. "Comparative Performance of Convolutional Neural Network, Weighted and Conventional Support Vector Machine and Random Forest for Classifying Tree Species Using Hyperspectral and Photogrammetric Data." *GIScience & Remote Sensing* 57 (3): 369–394. https://doi.org/10.1080/15481603.2020.1712102.

Stocker, T., Q. Dahe, K. Plattner, M. Tignor, S. Allen, and J. Boschung. 2013. *Climate Change 2013: The Physical Science Basis, Contribution of Working Group I to the Fifth Assessment Report of the Intergovernmental Panel on Climate Change*. Cambridge: Cambridge University press.

Su, Y., Q. Guo, B. Xue, T. Hu, O. Alvarez, S. Tao, and J. Fang. 2016. "Spatial Distribution of Forest Aboveground Biomass in China: Estimation Through Combination of Spaceborne Lidar, Optical Imagery, and Forest Inventory Data." *Remote Sensing of Environment* 173:187–199. https://doi.org/10.1016/j.rse.2015.12.002.

Tang, S., Y. Li, and Y. Wang. 2001. "Simultaneous Equations, Error-In-Variable Models, and Model Integration in Systems Ecology." *Ecological Modelling* 142 (3): 285–294. https://doi.org/10.1016/S0304-3800(01)00326-X.

Tao, S., F. Wu, Q. Guo, Y. Wang, W. Li, B. Xue, X. Hu, et al. 2015. "Segmenting Tree Crowns from Terrestrial and Mobile LiDAR Data by Exploring Ecological Theories." *Isprs Journal of Photogrammetry & Remote Sensing* 110:66–76. https://doi.org/10.1016/j.isprsjprs.2015.10.007.

Wang, G., T. Oyana, M. Zhang, S. Adu-Prah, S. Zeng, H. Lin, and J. Se. 2009. "Mapping and Spatial Uncertainty Analysis of Forest Vegetation Carbon by Combining National Forest Inventory Data and Satellite Images." *Forest Ecology & Management* 258 (7): 1275–1283. https://doi.org/10.1016/j.foreco.2009.06.056.

Xi, Y., C. Ren, Q. Tian, Y. Ren, X. Dong, and Z. Zhang. 2021. "Exploitation of Time Series Sentinel-2 Data and Different Machine Learning Algorithms for Detailed Tree Species Classification." *IEEE Journal of Selected Topics in Applied Earth Observations & Remote Sensing* 14:7589–7603. https://doi.org/10.1109/JSTARS.2021.3098817.

Xu, D., H. Wang, W. Xu, Z. Luan, and X. Xu. 2021. "LiDAR Applications to Estimate Forest Biomass at Individual Tree Scale: Opportunities, Challenges and Future Perspectives." *Forests* 12 (5): 550. https://doi.org/10.3390/f12050550.

Xu, Q., A. Man, M. Fredrickson, Z. Hou, J. Pitkänen, B. Wing, C. Ramirez, B. Li, and J. A. Greenberg. 2018. "Quantification of Uncertainty in Aboveground Biomass Estimates Derived from Small-Footprint Airborne LiDAR." *Remote Sensing of Environment* 216:514–528. https://doi.org/10.1016/j.rse.2018.07.022.

Yang, Q., C. Niu, X. Liu, Y. Feng, Q. Ma, X. Wang, H. Tang, and Q. Guo. 2023. "Mapping High-Resolution Forest Aboveground Biomass of China Using Multisource Remote Sensing Data." *GIScience & Remote Sensing* 60 (1): 2203303. https://doi.org/10.1080/15481603.2023.2203303.

Zald, H. S. J., M. A. Wulder, J. C. White, T. Hilker, T. Hermosilla, G. W. Hobart, and N. C. Coops. 2016. "Integrating Landsat Pixel Composites and Change Metrics with Lidar Plots to Predictively Map Forest Structure and Aboveground Biomass in Saskatchewan, Canada." *Remote Sensing of Environment* 176:188–201. https://doi.org/10.1016/j.rse.2016.01.015.

Zhang, N., X. Chai, N. Li, J. Zhang, and T. Sun. 2023. "Applicability of UAV-Based Optical Imagery and Classification Algorithms for Detecting Pine Wilt Disease at Different Infection Stages." *GIScience & Remote Sensing* 60 (1): 1. https://doi.org/10.1080/15481603.2023.2170479.

Zhang, Y., S. Liang, and G. Sun. 2014. "Forest Biomass Mapping of Northeastern China Using GLAS and MODIS Data." *IEEE Journal of Selected Topics in Applied Earth Observations & Remote Sensing* 7 (1): 140–152. https://doi.org/10.1109/JSTARS.2013.2256883.

Zhang, Y., J. Ma, S. Liang, X. Li, and J. Liu. 2022. "A Stacking Ensemble Algorithm for Improving the Biases of Forest Aboveground Biomass Estimations from Multiple Remotely Sensed Datasets." *GIScience & Remote Sensing* 59 (1): 234–249. https://doi.org/10.1080/15481603.2021.2023842.

Zhao, M., J. Yang, N. Zhao, Y. Liu, and T. Yue. 2019. "Estimation of China's Forest Stand Biomass Carbon Sequestration Based on the Continuous Biomass Expansion Factor Model and Seven Forest Inventories from 1977 to 2013." *Forest Ecology & Management* 448:528–534. https://doi.org/10.1016/j.foreco.2019.06.036.

Zhao, X., Q. Guo, Y. Su, and B. Xue. 2016. "Improved Progressive TIN Densification Filtering Algorithm for Airborne LiDAR Data in Forested Areas." *Isprs Journal of Photogrammetry & Remote Sensing* 117:79–91. https://doi.org/10.1016/j.isprsjprs.2016.03.016.

Zhao, Y., Y. Hao, Z. Zhen, and Y. Quan. 2017. "A Region-Based Hierarchical Cross-Section Analysis for Individual Tree Crown Delineation Using ALS Data." *Remote Sensing* 9 (10): 1084. https://doi.org/10.3390/rs9101084.

Zhao, Y., J. Im, Z. Zhen, and Y. Zhao. 2023. "Towards Accurate Individual Tree Parameters Estimation in Dense Forest: Optimized Coarse-To-Fine Algorithms for Registering UAV and Terrestrial LiDAR Data." *GIScience & Remote Sensing* 60 (1). https://doi.org/10.1080/15481603.2023.2197281.

Zhao, Y., Y. Ma, L. J. Quackenbush, and Z. Zhen. 2022. "Estimation of Individual Tree Biomass in Natural Secondary Forests Based on ALS Data and WorldView-3 Imagery." *Remote Sensing* 14 (2): 271. https://doi.org/10.3390/rs14020271.

Zhen, Z., L. Quackenbush, and L. Zhang. 2014. "Impact of Tree-Oriented Growth Order in Marker-Controlled Region Growing for Individual Tree Crown Delineation Using Airborne Laser Scanner (ALS) Data." *Remote Sensing* 6 (1): 555–579. https://doi.org/10.3390/rs6010555.

Zhen, Z., L. Yang, Y. Ma, Q. Wei, H. Jin, and Y. Zhao. 2022. "Upscaling Aboveground Biomass of Larch (Larix Olgensis Henry) Plantations from Field to Satellite Measurements: A Comparison of Individual Tree-Based and Area-Based Approaches." *GIScience & Remote Sensing* 59 (1): 722–743. https://doi.org/10.1080/15481603.2022.2055381.

Zolkos, S. G., S. J. Goetz, and R. Dubayah. 2013. "A Meta-Analysis of Terrestrial Aboveground Biomass Estimation Using Lidar Remote Sensing." *Remote Sensing of Environment* 128:289–298. https://doi.org/10.1016/j.rse.2012.10.017.

Appendix

Abbreviation list

ABA	area-based approach
AGB	aboveground biomass
ALS	airborne laser scanning
CNN	Convolutional neural networks
ITA	individual tree-based approach
ITCD	individual tree crown delineation
MC	Monte Carlo simulations
NSE	nonlinear simultaneous equation
Resnet	residual network
RF	random forest
rRMSE	relative root mean square error
RMSE	root mean square error
ULS	unmanned aerial vehicle laser scanning
TSC	tree species classification
SVM	support vector machine
U-HSIs	UAV-borne hyperspectral images
U-TLS	Fused ULS-TLS